MULTI EXCITON GENERATION AND RECOMBINATION OF SEMICONDUCTOR NANOCRYSTALS: FUNDAMENTAL UNDERSTANDING AND APPLICATIONS

A THESIS
SUBMITTED TO THE DEPARTMENT OF ELECTRICAL AND ELECTRONICS ENGINEERING
AND THE GRADUATE SCHOOL OF ENGINEERING AND SCIENCE
OF BILKENT UNIVERSITY
IN PARTIAL FULFILLMENT OF THE REQUIREMENTS
FOR THE DEGREE OF
MASTER OF SCIENCE

By
Ahmet Fatih Cihan
July 2013

I certify that I have read this thesis and that in my opinion it is fully adequate, in scope and in quality, as a thesis for the degree of Master of Science.

Assoc. Prof. Dr. Hilmi Volkan Demir (Supervisor)

I certify that I have read this thesis and that in my opinion it is fully adequate, in scope and in quality, as a thesis for the degree of Master of Science.

Prof. Dr. Ayhan Altıntaş

I certify that I have read this thesis and that in my opinion it is fully adequate, in scope and in quality, as a thesis for the degree of Master of Science.

Assoc. Prof. Dr. Mehmet Bayındır

Approved for Graduate School of Engineering and Science:

Prof. Dr. Levent Onural
Director of Graduate School of Engineering and Science

ABSTRACT

MULTI EXCITON GENERATION AND RECOMBINATION OF SEMICONDUCTOR NANOCRYSTALS: FUNDAMENTAL UNDERSTANDING AND APPLICATIONS

Ahmet Fatih Cihan
M.S. in Electrical and Electronics Engineering
Supervisor: Assoc. Prof. Dr. Hilmi Volkan Demir

July 2013

Semiconductor nanocrystal quantum dots (QDs) have been found to be very promising for important application areas in optoelectronics and photonics. Their energy band-gap tunability, high performance band-edge emission, decent temperature stabilities, and easy material processing make the QDs attractive for these applications ranging from photovoltaic devices to photodetectors and lasers to light-emitting diodes. For these QDs, the concepts of multi exciton generation (MEG) and recombination (MER) have recently been shown to be important especially because they possibly enable efficiency levels exceeding unity using these QDs in various device configurations. However, understanding multi exciton kinetics in QD solids has been hindered by the confusion of MER with the recombination of carriers in charged QDs. This understanding lacks to date and the spectral-temporal aspects of MER still remain unresolved in solid QD ensembles. In this thesis, we reveal the spectral-temporal behavior of biexcitons (BXs) in the presence of photocharging using near-unity quantum yield core/shell CdSe/CdS QDs. The spectral behavior of BXs and that of excitons (Xs) were obtained for the QD samples with different core sizes, exhibiting the strength-tunability of the X-X interaction energy in these QDs. The extraction of spectrally resolved X, BX, and trion kinetics, which would be spectrally unresolved using conventional approaches, is enabled by our approach introducing the integrated time-resolved fluorescence. Besides the fundamental

understanding of MEG and MER concepts, we also explored the possibility of utilizing multi excitons in these QDs for optical gain. In this part of the thesis, tunable, high performance, two-photon absorption (TPA) based amplified spontaneous emission (ASE) from the same QDs is presented. Here, for the first time, in addition to the absolute spectral tuning of the ASE, on the single material system of CdSe/CdS, the relative spectral tuning of ASE peak with respect to spontaneous emission was demonstrated. With the core and shell size adjustments, it was shown that Coulombic X-X interactions can be tuned to be either attractive leading to the red-shifted ASE peak or repulsive leading to the blue-shifted ASE peak and that non-shifting ASE can be achieved with the right core-shell combinations. It was further found here that it is possible to obtain ASE at a specific wavelength from both Type-I-like and Type-II-like CdSe/CdS QDs. In addition to the CdSe/CdS QDs, we showed ASE and Type-tunability features on CdSe/CdS nanorods (NRs), which are particularly promising with their extremely high TPA cross-sections and independent emission/absorption tunabilities. In the final part of the thesis, we report the observation of MEG on CdHgTe QDs, for the first time in the literature, and a novel application of MEG concept in a photosensor device, one of the first examples of real-life photosensing application of MEG concept. We believe that the results provided in this thesis do not only contribute to the fundamental understanding of MEG and MER concepts in the QDs, but also pave the way for the utilization of these concepts in the QD-based lasers, photodetectors and photovoltaic devices.

Keywords: Nanocrystals, quantum dots, excitonics, multi exciton generation, multi exciton recombination, amplified spontaneous emission, photosensors, lasers.

ÖZET

YARIİLETKEN NANOKRİSTALLERDE ÇOKLU EKSİTON OLUŞTURMASI VE YENİDEN BİRLEŞİMİ: TEMEL BİLİMSEL ANLAMA VE UYGULAMALAR

Ahmet Fatih Cihan
Elektrik ve Elektronik Mühendisliği Bölümü Yüksek Lisans
Tez Yöneticisi: Doç. Dr. Hilmi Volkan Demir

Temmuz 2013

Yarı iletken nanokristal kuvantum noktacıklarının (QD) optoelektronik ve fotonik alanlarındaki önemli uygulamalar için gelecek vaad eden malzeme sistemleri oldukları gösterilmiştir. Enerji bant aralığı ayarlanabilirliği, yüksek performanslı bant kenarı ışıması, uygun sıcaklık istikrarı ve kolay malzeme işlenebilirliği özellikleri QD'leri fotovoltaikten fotodetektörlere, lazerlerden ışık yayan diyotlara kadar birçok alanda cazip kılmaktadır. Yine yakın zamanda, bu QD'lerin bazı aygıt konfigürasyonları ile % 100 olan verimlilik sınırını aşabilme olasılığı sebebiyle, QD'lerde çoklu eksiton oluşturması (MEG) ve yeniden birleşimi (MER) konularının önemli olduğu gösterildi. Ancak QD katılarında çoklu eksiton kinetiklerinin anlaşılması MER ile yüklenmiş QD'lerdeki yeniden birleşme olayının karıştırılması sebebiyle zorlaşmış ve MER'nin spektral ve zamana bağlı özellikleri QD katılarında henüz tam çözümlenememiştir. Bu tezde, % 100'e yakın kuvantum verimliliğine sahip CdSe/CdS QD'lerde çift-eksitonların (BX) ve tek-eksitonların (X) spektral davranışlarını foto-yüklenme olayının varlığında açıklığa kavuşturduk. BX'lerin ve X'lerin spektral davranışlarını farklı çekirdek büyüklüğüne sahip QD örneklerinde elde ettik ve bu gözlemlerimiz QD'lerdeki X-X etkileşim enerjisinin şiddetinin ayarlanabilirliği özelliğini açığa çıkardı. Mevcut metotlarla mümkün olamayacak olan bu X, BX ve triyon yapılarının spektral olarak ayırt edilmesini,

entegre zamanda-çözümlenmiş floresans kavramını ortaya atarak başardık. MEG ve MER kavramlarının temel anlama konusuna ek olarak, çoklu eksitonların QD'lerde optik kazanım çalışmalarında yararlanılması konusunu da inceledik. Tezin bu kısmında, aynı QD'lerde spektral olarak ayarlanabilir, yüksek başarımlı, 2-foton soğurma (TPA) tabanlı yükseltilmiş kendiliğinden ışıma (ASE) çalışmamız özetlenmektedir. Burada, mutlak spektral ASE ayarlanabilirliğine ek olarak, CdSe/CdS malzeme sisteminde spektral ASE tepesinin olağan kendiliğinden ışıma tepesine göre bağıl olarak ayarlanabilirliğini literatürde ilk defa gösterdik. QD'lerin çekirdek ve kabuk boyutlarının ayarlanarak, Kulomb tipi X-X etkileşimlerinin kırmızı tarafa kayan ASE'ye sebep olan çekici veya mavi tarafa kayan ASE'ye sebep olan itici olarak ayarlanabileceğini gösterdik. Hatta doğru QD boyutlarıyla olağan kendiliğinden ışıma tepesiyle aynı spektral yerde ASE elde edilebileceği de bu kısımda gösterildi. Belli bir dalga boyunda elde edilen ASE davranışının tip-I veya tip-II olabilmesinin kontrolünün de mümkün olduğunu tezin bu bölümünde gösterdik. Tezin sonraki kısmında, CdSe/CdS QD'lara ek olarak, benzer ASE ve tip-ayarlanabilirliği çalışmasını, çok yüksek TPA soğurma ve birbirinden bağımsız soğurma/ışıma ayarlanabilirliği özellikleri ile dikkat çeken CdSe/CdS nanoçubuklarda (NR) da başarıyla gözlemledik. Tezin son kısmında MEG olayını CdHgTe QD'lerde ilk defa gösterdiğimiz deney sonuçlarımızı ve MEG kavramından, literatürdeki ilk örneklerden biri olarak, gerçek hayatta kullanılabilecek fotodetektör uygulamasında faydalanma çalışmamızı paylaştık. İnanıyoruz ki, bu tezde paylaşılan sonuçlar MEG ve MER kavramlarının temel anlaşılma yönüne katkı yapmakla kalmayıp bu kavramların QD lazerler, fotodetektörler ve fotovoltaik uygulamalarında da kullanılabilmeleri konusunda yeni gelişmelere yol açacaktır.

Anahtar Kelimeler: nanokristaller, kuvantum noktacıkları, eksitonlar, çoklu eksiton oluşturması ve yeniden birleşimi, yükseltilmiş kendiliğinden ışıma, fotoalgılayıcılar, lazerler.

Acknowledgements

Everything began when little Fatih stepped into the office of Prof. Demir in the early summer of 2010. That day, the meeting between Fatih and Volkan went extremely “positive” and the foundations of the relationship that will later turn out to be one of the most critical academic career steps of little Fatih were laid down. Since that day, Prof. Demir has always “kept up” with his motivational, encouraging, “supportive”, and positive approach towards Fatih training him on not only technically but also in terms of the political side of the science world. With Volkan’s efforts and contributions, Fatih has learned how to do world-class science and, hence, he is not as little as he was once.

I, as Fatih, would like to express my deepest gratitude to my MS thesis advisor Prof. H. Volkan Demir, who also supported me for my next career steps after Bilkent, besides his invaluable contributions to my academic development as mentioned above.

I would also like to thank my thesis committee members, Prof. Ayhan Altıntaş and Prof. Mehmet Bayındır. Their critical comments and feedbacks were very important for my thesis work.

I believe, one of the most important sides of working in Demir Group has been its members, which made coming to the office and lab much more enjoyable. As my office mates, Dr. Emre Sarı, Can Uran, Aydan Yeltik, Talha Erdem, Burak Güzeltürk, Kıvanç Güngör, Shahab Akhavan, Yusuf Keleştemur, İbrahim Akçalı, Halil Akçalı, Mehmet Zafer Akgül, and Onur Erdem each deserved separate acknowledgement pages. I should also thank Dr. Evren Mutlugün, Dr. Pedro L. Hernandez-Martinez, Dr. Sedat Nizamoğlu, Dr. Gökçe Küçükayan, Dr.

Nihan Kosku Perkgöz, Dr. Rohat Melik, Dr. Urartu Ö. Ş. Şeker, Dr. Vijay Kumar Sharma, Özgün Akyüz, and Emre Ünal for their friendly support during my MS degree. Also, I would like to express my thanks to the former and other group members Cüneyt Eroğlu, Muammer Yasin Hacısalihoğlu, Togay Amirahmadov, Somayeh Fardindoost, and Yasemin Coşkun.

Finally, I want to thank my family for their endless support, which is crucial for a junior researcher to survive in the academia. They have always been the number one source for me to solve the problems I have been facing.

I would also like to acknowledge the financial support I received from TUBİTAK BİDEB 2210 Program.

Table of Contents

List of Figures

List of Tables

Chapter 1

Introduction

Addressing the world's increasing energy demand has become one of the main goals of the scientific community in the past decades. The super-linear increase in energy need of the world has enforced the energy production to be increased accordingly. However, the traditional fossil fuel usage as the energy source cannot follow the extreme rate at which the energy demand increases because of the fossil fuels' CO_2 emission that Earth can no longer manage to tolerate. At this point, the concept of renewable energy has arisen as one of the solutions to future energy problem.

One of the most promising renewable energy methods is solar energy about which the fields of photonics and optoelectronics are critically important. This is mainly because, with the necessary advances in these fields, the conversion of the sun light energy to electricity will become more and more efficient, which is an essential development for the solar energy systems to become a significant energy source. Within this context, recently emerging concept of multi exciton generation (MEG), generation of multiple excitons upon absorption of single photon, has the promise to enable a significant efficiency improvement in photovoltaics [1]. By utilizing the extra energy of the incoming photon above the bandgap of the semiconductor absorber material to excite a second valence band electron across the bandgap, MEG phenomenon can potentially be used to obtain solar cells exceeding the famous Shockley-Queisser thermodynamic limit [2–13]. Indeed, it has recently been shown that with the proper utilization of

MEG concept, even above 100% external quantum yield on solar cells is possible [14].

The most promising material system for obtaining high performance MEG feature has been shown to be semiconductor nanocrystal quantum dots (QDs) because of phonon bottleneck (inhibition of phonon emission in QDs because of discretized energy levels), enhanced Coulomb interactions due to strong electronic confinements, and relaxation of translational momentum conservation in QDs [5,10,15–18]. Absence of these features in the bulk counterparts of semiconductor QDs encouraged researchers to explore MEG in QDs.

Although there has been a tremendous effort on understanding the concepts of MEG and multi exciton recombination (MER) in QDs, a lot of contradicting results were reported in the literature about the efficiency of these processes and the physics behind them. Especially the confusion of the recombination behaviors of multi excitons with the recombination in charged QDs has been an important issue to resolve. The first part of this thesis is about this issue: the scientific understanding we developed about the extraction of spectral and temporal behaviors of multi excitons, charged excitons (trions), and single excitons in QDs.

The other important research area that relies on MEG and MER processes is the utilization of QDs as the gain medium for lasing applications [19,20–23]. The emission wavelengths of conventional laser systems are dictated by the atomic transitions of the active materials used in these systems. Therefore, unless very complicated nonlinear processes are involved, it is not possible to obtain lasing action in every spectral position we require using the conventional active gain medium materials. At this point, QDs stand out as freely tunable material systems that have the potential to provide lasing at any wavelength desired in

principle when properly tuned. Therefore, the spectral tunability feature of QDs makes them very promising candidates for lasing applications. A very recent demonstration of vertical cavity laser employing QDs as active gain medium is a very good example of how QDs can revolutionize the current laser technology [22]. In this thesis, we present our results on how we can master the amplified spontaneous emission (ASE) with both absolute spectral tunability and relative one with respect to spontaneous emission. The high performance ASE is observed for differently sized core/shell QDs and NRs and the experiments using nanocrystals with different sizes and shapes revealed the tunability of exciton-exciton interactions in these material systems.

Another field that has the potential of benefiting from MEG concept is photodetection. With the presence of MEG event in photodetectors, the photodetection efficiency can be improved significantly because of the possibility of generating a second electron while the conventional structures lose the energy for the second electron as heat dissipation. Within this context, the most commonly used near-infrared and infrared emitting QDs on MEG and MER studies are PbSe and PbS QDs [7,16,24–28]. Although CdHgTe QDs can be very good near infrared alternatives considering the fact that CdHgTe is a material that has already been employed as commercial photodetection material, CdHgTe QDs have not been considered for MEG-photodetection applications [29]. In this thesis, we demonstrated MEG, for the first time, from CdHgTe QDs and as one of the first real-life utilizations of MEG concept, we employed MEG concept on CdHgTe QD-based photosensors.

We believe that from fundamental understanding to practical utilization, we provide a comprehensive MEG and MER study on QDs in this thesis. Our findings do not only clarify some of the significant controversies in the literature on MEG/MER, but also show new ways of exploiting multi excitons in lasers

and photodetectors. This thesis hopefully also helps the MEG and MER phenomena become more feasible in real-life applications through the new scientific understanding, proposed approaches and novel engineering perspectives it provides.

This thesis work is organized as follows:

In Chapter 2, after this introductory chapter, we provide brief necessary background information on QDs, MEG, MER and ASE phenomena.

In Chapter 3, the method of extraction of spectral and temporal behaviors of multi excitons in the presence of photocharging effect in CdSe/ CdS QDs is presented and the results are discussed. This chapter includes various independent experimental verifications of the comments and claims about the resolution of different excitonic events taking place in the QD ensembles. Here we also discuss the dependences of spectral behaviors of various excitonic events on QD core sizes.

In Chapter 4, we discuss the experimental results on ASE behavior of CdSe/CdS QDs pumped with a two-photon absorption (TPA) mechanism. We firstly provide experimental supporting evidence for the claim that the CdSe/CdS QDs have one of the best TPA cross-sections among many other alternatives. It is this chapter where we report the first demonstration of both blue- and red-shifted ASE with respect to regular spontaneous emission from different-size QDs (Type-tunability feature). In the second part of this chapter, similar to the first part, we provide our results on the Type-tunability feature of CdSe/CdS nanorods (NRs) in their ASE feature. The Type attributions of different NRs are verified by independent time-resolved fluorescence experiments.

In Chapter 5, we present the results on the demonstration of MEG on CdHgTe QDs and the utilization of MEG concept on photosensors employing CdHgTe QDs. Here, we report the clear sensitivity enhancement of the photodetector for the incoming photon energies for which MEG event is possible.

In Chapter 6, we conclude our discussions and summarize our scientific contributions as the results of the thesis works presented here.

Chapter 2

Scientific Background

2.1 Semiconductor Nanocrystal Quantum Dots and Nanorods

2.1.1 Excitonic Structure and Optical Properties of Quantum Dots

QDs are semiconductor nanocrystals that consist of several hundreds to several thousand atoms reaching about a couple of nanometers in size. The colloidal QDs are the ones that we focus on in this thesis work. In order to avoid the QDs in the ensemble to come and stick together, the colloidal QDs are coated with organic (for QDs dissolved in organic solvents) or inorganic ligands (for QDs dissolved in inorganic solvents).

The most interesting feature of QDs making them very promising in a lot of application areas from photovoltaics to photodetectors and lasers to light emitting diodes is that their energy bandgap can be adjusted by just changing their sizes because of the "Quantum confinement effect". This effect is strong in QDs when the exciton Bohr radius is smaller than the dimensions of the QDs, the regime called strong confinement regime. In this case, it can be said that electron and hole are tightly confined by the energy barrier surrounding the QD in all three dimensions. With this effect, as the QD size gets smaller, the discretization of energy levels of the QD becomes stronger and the bandgap becomes larger, which is illustrated in Figure 2.1.1.1. As can be seen on the following equation, as the radius of the QD decreases, the bandgap increases:

$$E_g(QD) \approx E_{g,bulk} + \frac{\hbar^2 \pi^2}{2 m_{e/h} R^2} \tag{2.1}$$

where, $E_g(QD)$ is the bandgap of QD, $E_{g,bulk}$ is the bandgap of the bulk form of the semiconducting material, $\hbar$ is the reduced Planck constant, $m_{e/h}$ is the electron/hole effective mass, and R is the radius of the QD.

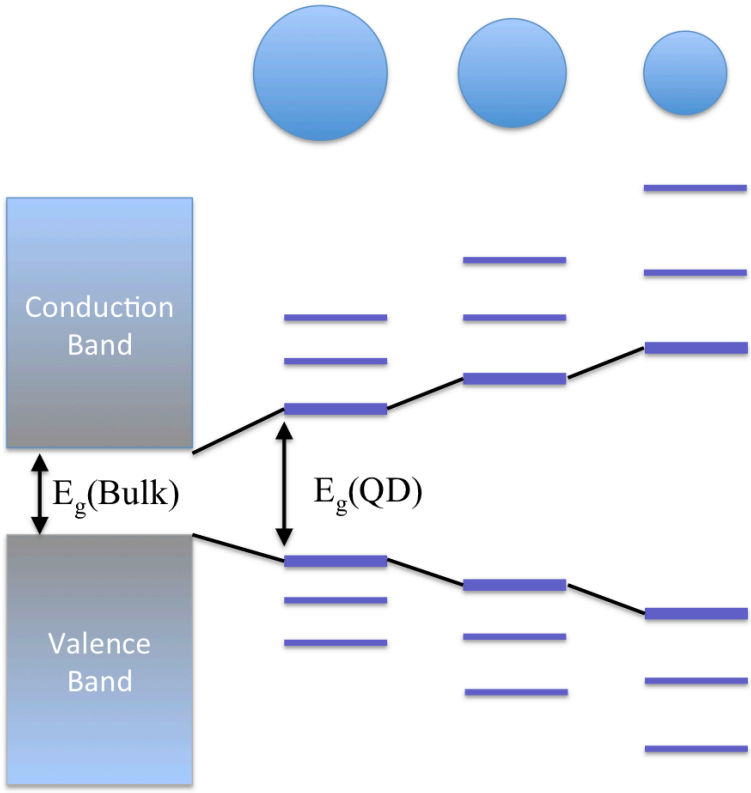

Figure 2.1.1.1. Discretization of energy levels as the QD size gets smaller.

The resulting bandgap tunability of QDs can also be seen in their photoluminescence emission behaviors as shown in Figure 2.1.1.2.

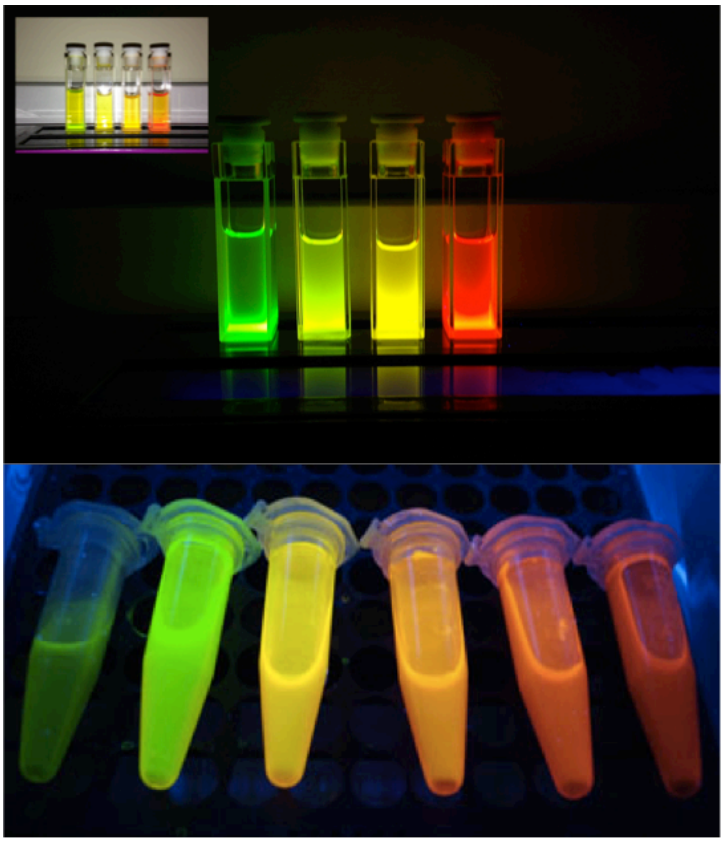

Figure 2.1.1.2. Color tunability of QDs with different sizes under ultraviolet light.

Coating the QDs with a different semiconductor material having a certain thickness adds another degree of freedom on the excitonic engineering possibilities of QDs. This kind of structure is called core/shell structure and the mostly used QDs in this work are of this kind. The schematic illustration of this type of QDs with the representative energy band diagram is given in Figure 2.1.1.3.

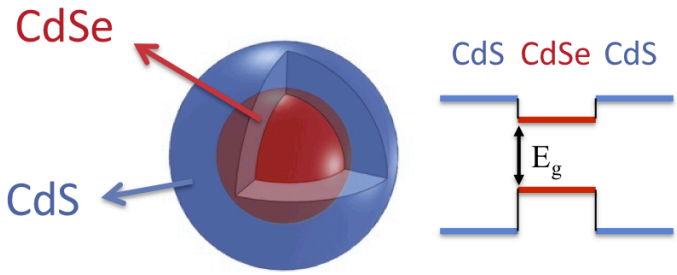

Figure 2.1.1.3. CdSe/CdS core/shell QD (left) and its energy band diagram (right).

There are three different core/shell QD types: Type-I, Type-II and quasi-Type-II. If the electron and hole are confined in the same part of the QD (core or shell), the QD is called Type-I. If the electron and hole are localized at different position of the QD, the excitonic type of the QD is Type-II. However, if the electron and hole wavefunction overlap is partial, as is the case for CdSe/CdS QDs, the QD is called to be quasi-Type-II.

Besides the core/shell CdSe/CdS QDs, we employed also NRs of the same material system of CdSe/CdS in our optical gain studies in this thesis work. The representative shape of CdSe/CdS NRs is provided in Figure 2.1.1.4. There are two main differences between QDs and NRs used here. The first one is the obvious shell size and shape difference where NRs have an elongated CdS shell leading to extremely high absorption cross-section values. The second difference is that NRs have a lower photoluminescence quantum yield (less than 50%) compared to the near unity quantum yield of QDs. This quantum yield difference is due to the synthesis method difference and the reduced electron/hole wavefunction overlap in NRs as a result of the reduced quantum confinement effect.

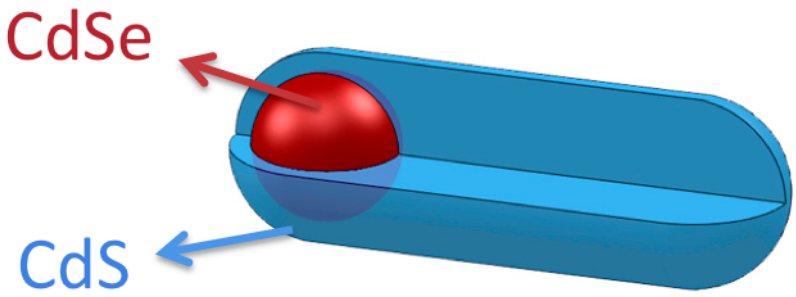

Figure 2.1.1.4. CdSe/CdS NRs used in this work.

2.1.2 Synthesis of Quantum Dots

The synthesis of core/shell QDs basically consists of a two-step process: synthesis of the core QDs and shell coating of these QDs. Since CdSe/CdS QDs are the ones that we used most in this thesis work, we will provide the synthesis basics and procedure for the synthesis of CdSe/CdS QDs.

2.1.2.1 Synthesis of CdSe Core QDs

The core CdSe synthesis is based on the discrete nucleation of CdSe molecules in a well-defined crystal structure upon the supersaturation of synthesis environment with Cd and Se precursors. After the injection of the precursors to the hot coordinating solvent, the nucleation takes place and to stop the nucleation phase, the temperature should be decreased immediately after the necessary time passes.

The core synthesis method we used in this work is similar to the reports in the literature [30,31]. First, in a three-neck flask, 96 mg of CdO, 450 mg of Tetradecylphosphonic acid (TDPA, 98%) and 6 g of trioctylphosphine oxide (TOPO, 90%) are mixed and the temperature is elevated to 130-150°C under

vacuum. Then the temperature is elevated to 350°C under argon atmosphere. While this solution is being kept under this condition for about 1 hour, 3.3 mL tributylphophine-Se (TBP-Se) (1.5 M) precursor is prepared by mixing 4.95 mmol Se with 3.3 mL of TBP in a glovebox. Then, after making sure that CdO is totally dissolved and the solution in the flask became totally transparent, the temperature is lowered to 273°C and the Se precursor is injected. Immediately after the TBP-Se injection, the system is brought to room temperature to stop the growth of the cores.

Figure 2.1.2.1.1. Glove box system used for the handling of chemicals that are sensitive to oxygen environment.

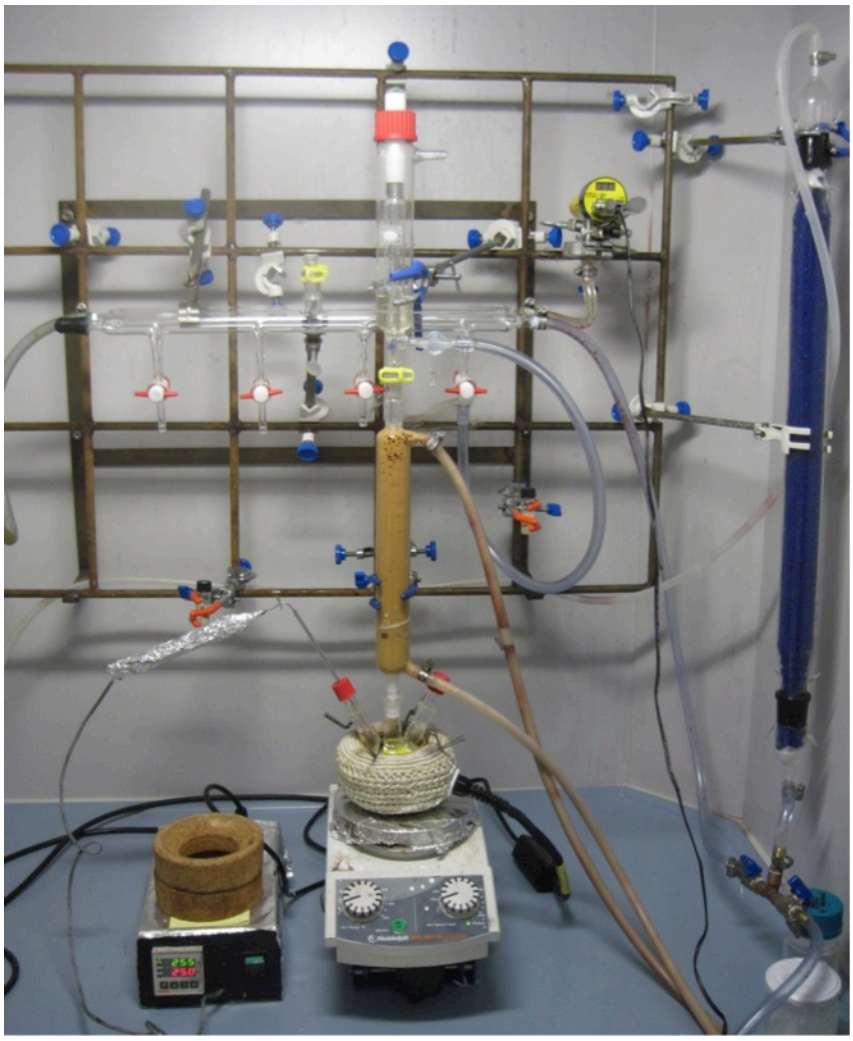

Figure 2.1.2.1.2. CdSe core synthesis setup with a three-neck flask, a temperature controller, a pressure gauge, and a Schlenk line in fume hood.

2.1.2.2 CdS Shell Coating of CdSe Cores with SILAR Technique

The synthesis of CdSe/CdS QDs having a core radius of ca. 1.22 nm and a shell thickness of ca. 1.4 nm was carried out through modified selective ion layer adsorption and reaction (SILAR) technique as Greytak et al. previously reported [32,33].

After the preparation of CdSe cores as described in the previous part, we prefer to keep the CdSe core QDs in a fridge overnight which later makes it easier to clean the solution from residual materials. For the Cd precursor preparation, Cd-oleate (2.5 mL), oleylamine (0.3 mL) and trioctylphophine (TOP) (2.2 mL) are mixed in the glovebox. After this process, some more TOP and oleylamine are added to make the Cd concentration 0.1 M. For S precursor, 105 μL $(TMS)_2S$ is mixed with 4.9 mL of TOP to obtain 0.1 M S concentration in glove box.

After we obtain the Cd and S precursors, the core/shell QDs are synthesized using the recipe in the literature [32]. First, 6 mL of octadecene (ODE) and 3 mL oleylamine are mixed in a four-neck flask and the temperature is elevated to 100°C and kept under vacuum for 30 min. Then, the temperature is lowered to room temperature and the previously synthesized CdSe cores are injected into the flask. To evaporate the hexane in the solution, the system is kept under vacuum until no bubble formation resides. Subsequently, the temperature is increased to 180°C and a certain amount of prepared Cd precursor is injected into the flask with the help of a syringe pump slowly for 3 min. After Cd precursor injection, we wait for 12 min and then inject the S precursor similarly. Continuing in this alternating fashion between the Cd and S precursors, after reaching the 4^{th} CdS monolayer surrounding CdSe cores, we decrease the temperature to 80°C and keep the system at that temperature for annealing. After coming to room temperature, we add hexane to the solution and start the cleaning procedure. For cleaning, the sample is first centrifuged to get rid of the remaining unwanted residues. Then, acetone or methanol is added and the QDs precipitate. After the removal of the solution on top of the precipitated QDs, the QDs are dissolved in hexane.

Since the CdS shell layers were grown around the cores at 180°C, the formation of interfacial alloy layers of CdSeS is not expected in this synthesis. The size

distribution of the QDs obtained with this synthesis method is narrow (with a <10% deviation from the average QD size) as can be seen in the transmission electron microscopy image of the QDs given in Figure 3.1.1.1. The PL full-width at half-maximum value of *ca.* 25 nm also indicates the highly monodisperse size distribution of the QDs.

2.2 Multi Exciton Generation and Recombination

2.2.1 Description of Multi Exciton Generation and Recombination and Current State of the Field

Photogeneration and recombination of multi excitons (MEs) in semiconductor nanocrystal quantum dots have recently attracted significant scientific interest as a possible means to improve the performances of QDs in device applications. High surface quality and small density of defect sites with engineered band structures of recently developed core/shell QDs, especially the ones with core/shell materials of CdSe/CdS [19,32,34–38] and CdTe/CdSe [39–41], enabled better multi exciton generation and recombination performances encouraging researchers in this field. In very recent reports, MEG phenomenon has indeed been shown to be very promising especially for improving the solar energy conversion efficiencies [3,5,6,9,14,42–47]. It has also been demonstrated that even over 100% peak external quantum efficiency is possible for the QD solar cells exploiting the MEG concept [14]. Another important research area that relies on MEG and MER processes is the utilization of QDs as the gain medium for lasing applications [19,20–23]. Easy spectral tunability and comparatively easy synthesis of QDs via wet chemistry make them very convenient candidates for the lasing applications. In addition to photovoltaic and lasing applications, the MEG concept has also been shown to significantly improve the photodetector device performances [48]. For all of these application

areas, the most pronounced limiting effect is the nonradiative Auger recombination (AR) of MEs. Therefore, the suppression of AR is also under intense research in order to benefit from the MEs most effectively [19,35,37–39,49]. Until very recently, MER had been believed to be fully nonradiative as AR. However, it was shown that MERs do not have to be nonradiative and could even be made fully radiative for some special QDs [38,50].

MEs can be generated in a QD either by absorption of a highly energetic single photon followed by carrier multiplication (CM) process or by sequential absorption of multiple photons in a single pulse with lower photon energies [24]. As illustrated in Figure 2.2.1.1, we generated MEs using the latter method. Since the behavior of MEs generated by either method has been shown to be the same [51], the results presented in Chapter 3 of this thesis are valid also for the MEs generated by CM.

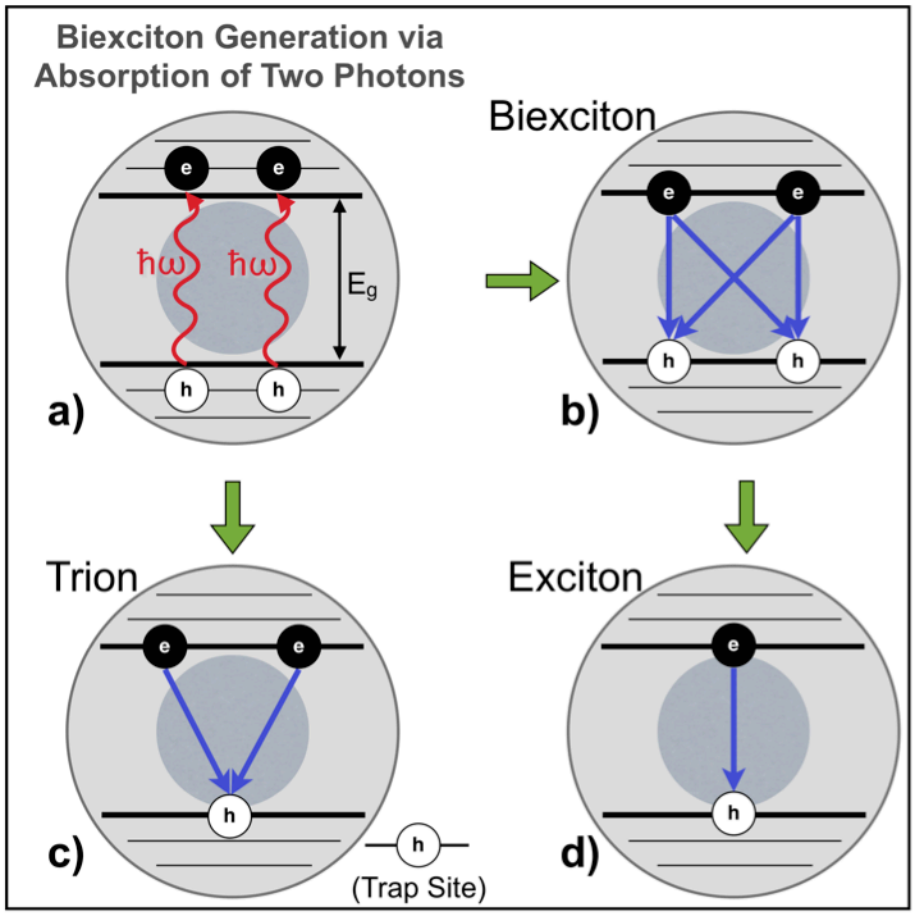

Figure 2.2.1.1. a) Biexciton generation in a QD via absorption of two photons with energies ħω. b) Biexciton formation immediately after the relaxation of excitons to the band edge. (The blue arrows indicate the possible recombination pathways.) c) Trion composed of a hole and two electrons. The other hole is trapped at a trap site of the QD. d) Exciton in a QD. This could be generated by direct absorption of a single photon or after the recombination of a BX. (The grey circles represent a core/shell QD. "e" denotes an electron and "h" denotes a hole. "E_g" stands for the bandgap energy of the QD.) (Reprinted with permission from Cihan et al. [1] Copyright 2013 American Chemical Society.)

This material combination of CdSe used as the core and CdS used as the shell has previously been shown to have a very good radiative MER behavior because of the suppression of AR in the case of "giant" QD structure, where the core is surrounded by at least 8-10 monolayers of CdS [19,35,38]. As will be discussed

in the next chapter, nonradiative AR is substantially suppressed (but not necessarily completely) in the QDs studied in this thesis work, the resulting MEs in a significant portion of QDs in the ensemble have performed radiative recombination similar to the MEs in the giant QDs reported with the same core/shell materials.

2.2.2 Scientific Challenges of Multi Exciton Generation and Recombination

Although there are a lot of strong experimental and theoretical studies in the literature on MEG using a wide variety of material and shape combinations, the temporal and spectral aspects of the generation and recombination of MEs still remain under debate. Especially the confusion of the MER with the recombination of carriers in a charged QD has caused a lot of different and contradicting results to be reported in the literature [5,51–55]. The confusion of the recombination in charged QDs and the MER has previously been addressed through the prevention of charging of the QDs by effectively exposing each QD to pulses of excitation less frequently through stirring or flowing the samples in solution [6,56–58]. Although this approach has led to very important explorations and clarifications about MEs, a deeper understanding of MEs is necessary because avoiding the photocharging of the QDs in practical applications, such as QD lasing and solar energy conversion based on MEG, where typically thin films of QDs are used in solid form, may not be generally possible. Therefore, the behavior of the MEs in the presence of photocharging in solid QD ensembles is still required to be well understood in order to fully utilize MEs in real life applications of solid-state devices. In the corresponding chapter of this thesis, we addressed this confusion of MER and recombination in charged QDs.

2.3 Time-Resolved Fluorescence Spectroscopy

Time-resolved fluorescence (TRF) spectroscopy is a very strong method that gives us the opportunity to observe, explore and understand the physical and chemical events taking place in the nanostructures of our interest. The type of TRF employed in our thesis work is time-correlated single photon counting (TCSPC). This method is a statistical method that is based on very high number of photon counting sub-experiments that constitute a statistical global decay behavior of the sample under test.

This method works in the following way: the pulsed laser source sends a pulse and excites the sample. Then, the sample emits a photon after a certain time depending on its quantum mechanical structure. The photomultiplier tube detects the photon and the electronic system records the time between the laser pulse generation and the sample's photon emission. This process is repeated millions of times and the histogram of the photons collected at each time instant is the result of the fluorescence decay of the sample under test. The TRF setup we used in our TCSPC measurements is provided in Figure 2.3.1.

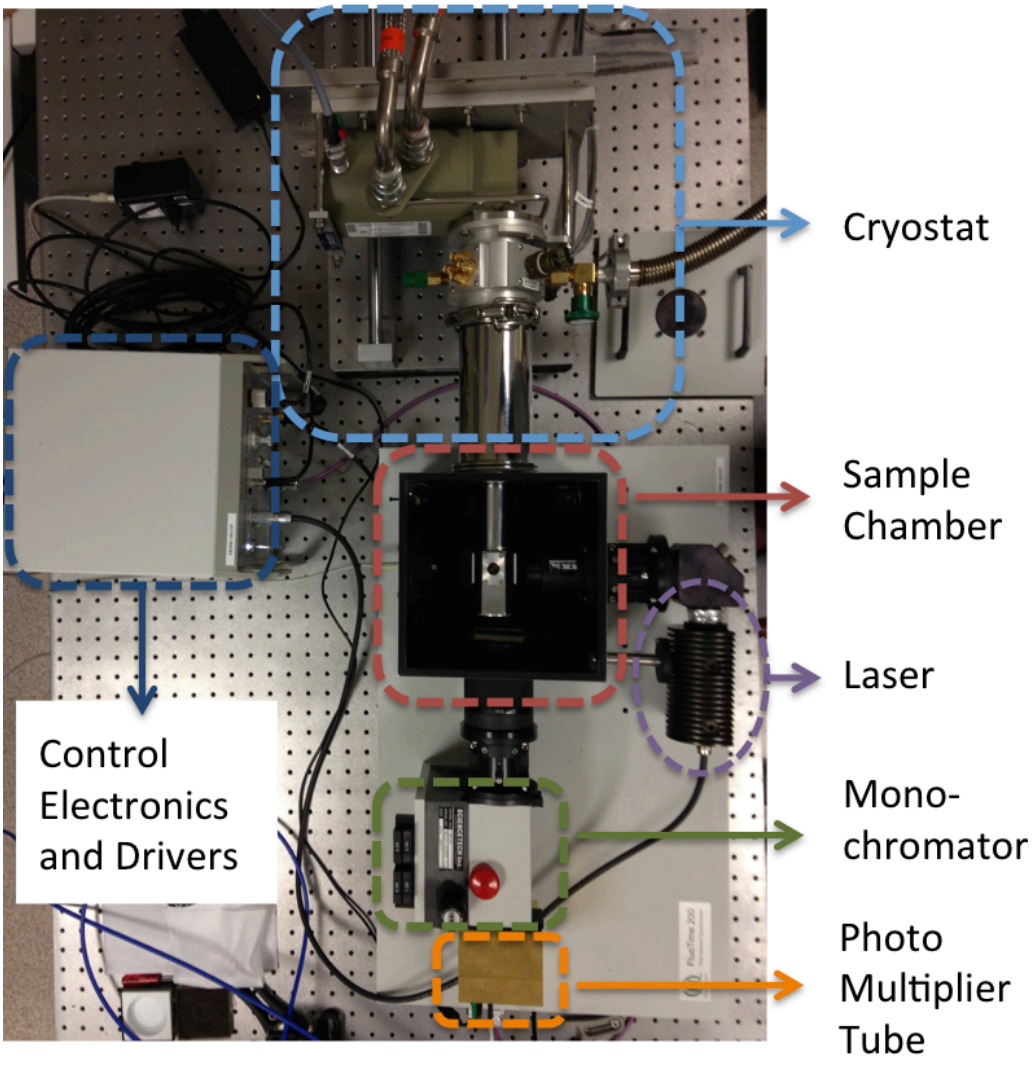

Figure 2.3.1. Time-resolved fluorescence setup with cryostat.

Chapter 3

Resolution of Biexcitons, Trions and Single Excitons in CdSe/CdS Core/Shell Quantum Dots

This chapter is based on the publication "Observation of biexcitons in nanocrystal solids in the presence of photocharging," A. F. Cihan, P. L. Hernandez-Martinez, Y. Kelestemur, E. Mutlugun, and H. V. Demir, *ACS Nano*, 7, 4799-4809 (2013). Reprinted with permission from American Chemical Society.

In this part of the thesis, we present the spectral-temporal behavior of biexcitons (BXs) in the presence of photocharging in near-unity quantum yield (QY) CdSe/CdS core/shell nanocrystals. By studying three QD samples with different core radii, we observe the spectral behavior modifications of the BXs as the result of strength tunability of X-X interactions in the CdSe/CdS QDs with size variation. Resolution of the recombination events of Xs, BXs and trions in our ensemble measurements was achieved with the TCSPC experiments under variable excitation intensities at different emission wavelengths. In order to extract X, BX, and trion decays, we developed an analysis approach for the time decays of the sample where we described the physical events happening in the QD ensemble with their corresponding time decay terms having specific lifetimes. This method, which uses the decay lifetime differences of different

events to discriminate other events, provides us with the ability to distinguish the spectral behaviors of Xs, BXs, and trions, even when their spectral behaviors are almost the same, by tracing the corresponding decay terms throughout the spectrum. As a result, the spectral radiative recombination kinetics of Xs, BXs, and trions were obtained. Moreover, we verified our results by crosschecking the excitation intensity dependences of these recombination events, evolutions of the photoluminescence spectra with time, independent steady-state photoluminescence behaviors, and exposure time dependences, all of which proved to be consistent with each other.

3.1 Experimental Details

3.1.1 CdSe/CdS Core/Shell Quantum Dots Used in the Experiments

The CdSe/CdS QDs used in MEG/MER experiments possess very high crystal quality and very narrow size distribution. The transmission electron microscopy (TEM) images in Figure 3.1.1.1 show a nearly perfect arrangement of QDs, which points toward the low size variance of QDs. PL emission and absorption spectra of QDs dispersed in hexane are provided in Figure 3.1.1.2.

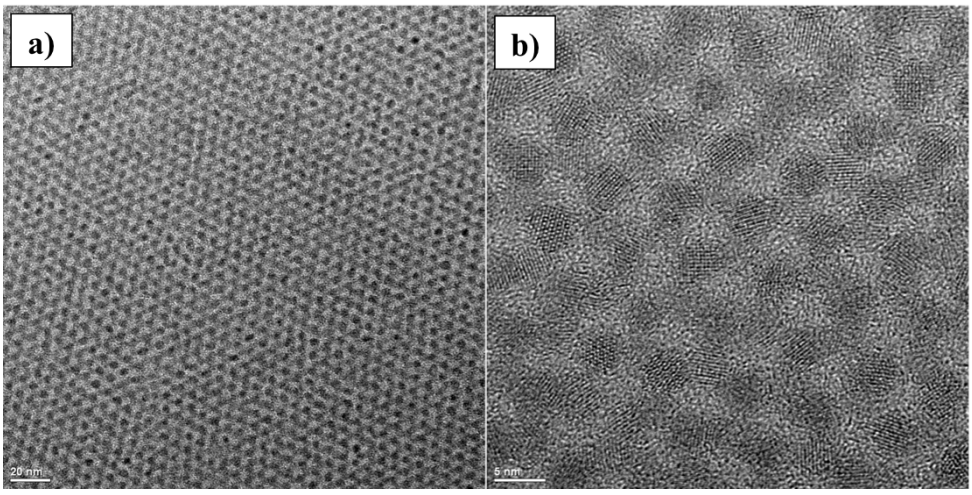

Figure 3.1.1.1. TEM images of CdSe/CdS QDs with a) 20 nm and b) 5 nm scale bar.

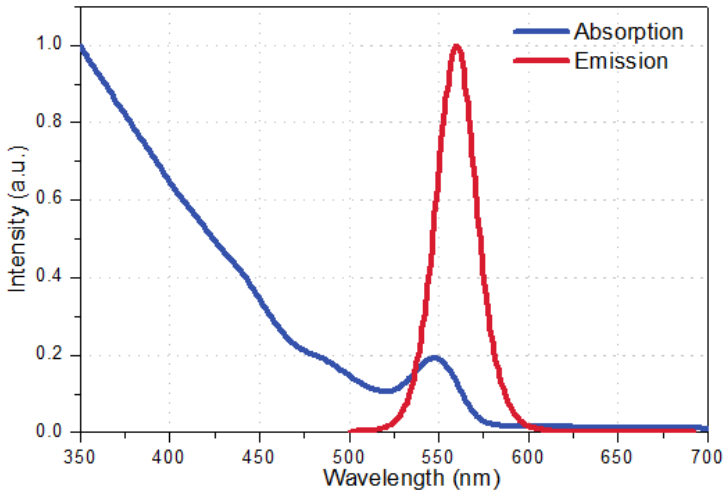

Figure 3.1.1.2. Photoluminescence emission and absorption spectra of CdSe/CdS QDs.

3.1.2 Sample Preparation

The CdSe/CdS core/shell QDs were dispersed at a medium concentration level in hexane. Then, 2 µL of the QD solution was mixed with 98 µL of Poly(methyl methacrylate) (PMMA) A7.5 with the help of a Vortex mixer (Velp Scientifica Inc.) for approximately 5 min until QDs were dispersed completely homogeneously inside the PMMA. 50 times dilution of the QD solution ensured the very low concentration of QD solids in PMMA, which allowed us to obtain very homogeneous QD distribution in the solid medium on the quartz substrate. Moreover, the Förster-type nonradiative energy transfer (NRET) among the QDs was suppressed because of the increased average inter-particle distance (>50 nm) and high dielectric surrounding medium. 25 µL of this QD-PMMA mixture was spin-coated onto clean quartz substrates of 1cm by 1cm in dimensions at a 1500 rpm rotation speed for 3 min.

3.1.3 Time-Resolved Fluorescence Experiments

We used a 3.3 eV (375 nm) pulsed laser excitation with a pulse width of <50 ps at a repetition rate of 5 MHz which is focused to a spot size of 37 μm^2 on the

sample for the TCSPC measurements (Picoquant Fluotime 200). Laser fluences were varied from 9.8×10^{12} to 5.1×10^{14} photons/cm^2 per pulse. The collection part of the TRF setup consists of a monochromator with 8 nm wavelength resolution and a 0.3 nm wavelength accuracy and a photomultiplier tube with controlling electronics resulting in a time resolution of ca. 200 ps. To avoid phonon-mediated undesired processes as much as possible, the experiments were conducted at temperatures below 20 K with the help of a closed cycle liquid He cryostat (Cryo Industries).

3.2 Extraction of Biexcitons, Trions and Single Excitons from Time-Resolved Fluorescence Decays of Quantum Dots

The experimental time-resolved fluorescence (TRF) results were analyzed by least chi-square fittings based on a multi-exponential fitting

$$A_1 e^{-t/\tau_1} + A_2 e^{-t/\tau_2} + A_3 e^{-t/\tau_3} + A_4 e^{-t/\tau_4} + Noise \tag{3.1}$$

without enforcing any specific lifetime in any of the analyses. Since the best chi-square values were obtained for the 4-exponential fittings, the decay curves were fitted with the four exponentials. Here it is also worth noting that we also checked the resulting spectral behaviors with three exponentials, which resulted in physically meaningless steep changes in the individual lifetime values for the varying emission wavelength. The consistency of the lifetime values and ratios of each decay term to each other throughout the entire spectrum, as provided in Figure 3.4.1, also justifies that each decay term represents a physical event. For the 5-exponential fitting trials, the fifth decay coefficient turned out to be zero justifying our 4-exponential fittings. The numerical fitting therefore identified the best matching sets of (A_i, τ_i). The fitting lifetime components of interest here are at least orders of magnitude longer than the excitation pulse width and the

instrument response function. Therefore, the results can be considered as the response of the system to an impulse excitation.

The method of extraction of X, BX, and trion recombination events from the total time decay curves of the ensemble is based on the lifetime differences of these physical events taking place in the ensemble. In other words, the kinetic signatures of the events are used to distinguish one from the other when exploring the spectral distributions and excitation intensity dependences of these events. Therefore, each one of the exponential decay terms in the fitting (Equation 3.1) can be attributed to a specific recombination event happening inside the QD ensemble. The resulting lifetimes together with their associated coefficients may then be examined to obtain the desired spectral dynamic behavior of the corresponding event. To find the total number of occurrences of a radiative recombination event in the ensemble, the total number of photons emitted from the sample should also be known. Integration of each decay term with respect to time gives the total number of photons emitted as a result of the corresponding physical event having that characteristic lifetime. Therefore, once the fitting coefficients and lifetimes are identified, the spectral distributions and excitation intensity dependences of the events happening in the excitation volume of the sample can conveniently be extracted and studied. Since we do not expect the emissions due to different events to have different angular emission dependences, the integration in Equation 3.2 can be considered as a sampling of the number of occurrences of the event represented by the decay term $A_i e^{-t/\tau i}$ (i=1, 2 or 3), which is simply equivalent to the product of the lifetime describing the specific event with its weighting coefficient. Mathematically speaking, it is then necessary to keep track of $A_i\tau_i$ as a function of emission wavelength, for each event i. Therefore, it is physically more meaningful to study and compare $A_i\tau_i(\lambda)$ spectra of different events, rather than $A_i(\lambda)$ for a specific τ_i.

$$\int A_i e^{-t/\tau_i} dt = A_i \tau_i \tag{3.2}$$

This kind of lifetime extraction methodology using TCSPC measurements has enabled us to resolve the spectral dynamic behaviors of different recombination events that would otherwise be unresolvable in ensemble systems with other methods that do not exploit the lifetime differences between the events. For example, in our case, we extracted the spectral dynamic behaviors of three different events taking place in the QD ensemble even though they are not distinguishable in the steady state PL measurements. Thus, this approach allows us to overcome the problems of inhomogeneous broadening of QD emissions when the spectral peak positions of the two events are very close to each other. With this method, the lifetimes of each event throughout the whole emission spectrum can be analyzed. Moreover, the spectral, temporal and power dependent behaviors of different events can further be obtained even when they are spectrally unresolvable in the ensemble system.

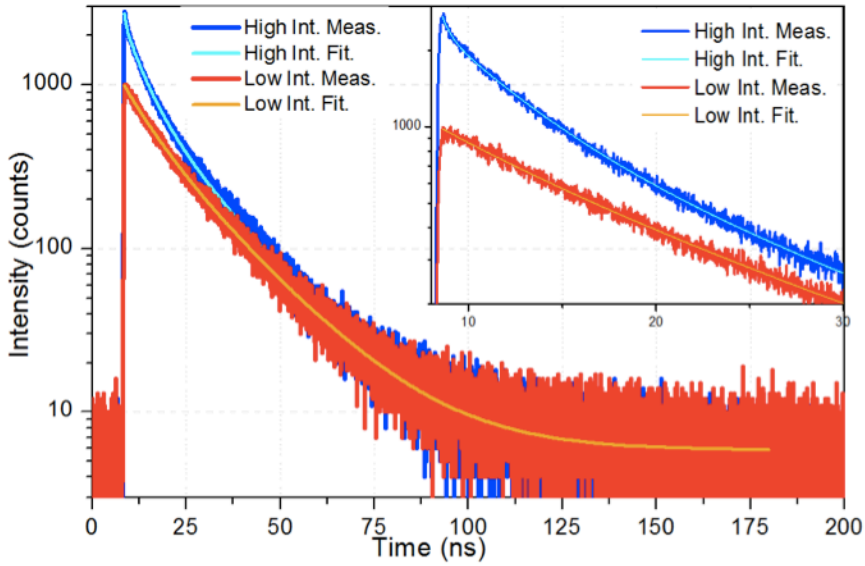

Figure 3.2.1. TRF decays and fittings of the QD solid sample under low (9.8×10^{12} photons/cm^2 per pulse and average number of absorbed photons per QD: $\langle N \rangle = J_p \sigma_{abs} = 0.03$, where J_p is the per pump photon fluence and σ_{abs} is the QD absorption cross-section) and high intensity (5.1×10^{14} photons/cm^2 per pulse, $\langle N \rangle = 1.43$) excitations collected for the same time duration given in red and blue curves, respectively. (inset) The first 30 ns segments of these time decays. (Reprinted with permission from Cihan et al. [1] Copyright 2013 American Chemical Society.)

Table 3.2.1. Fitting coefficients and lifetimes of high and low intensity excitation cases.

	A_1	τ_1 (ns)	A_2	τ_2 (ns)	A_3	τ_3 (ns)	A_4	τ_4 (ns)
Low Int.	530±13	18.4	372±26	8.31	73±36	4.60	-	-
High Int.	539±15	18.9	559±28	10.7	1218±5	4.44	404±214	0.41

Figure 3.2.1 shows the TRF decay curves taken at the photoluminescence peak of the QD solid sample for low and high intensity excitation cases. The emergence of the third and fourth exponential components for the high intensity excitation case can be seen here. The corresponding fitting coefficients and lifetimes are given in Table 3.2.1. After collecting the fluorescence decay curves of the QDs at all emission photon energies for the specific excitation intensities,

we obtain the spectral distributions of the coefficients of each exponential term in the overall decay (Equation 3.1).

The normalized fitting coefficients of each term in the overall decay for the medium intensity excitation case are shown in Figure 3.2.2(a), which is useful to observe the spectral shifts between the events. The coefficients are provided here in the normalized form because the absolute amplitudes of the coefficients themselves might be misleading due to the fact that one needs to take the lifetimes into account to properly calculate the number of photons emitted as a result of that event. For example, as can be seen in Figure 3.2.3, the coefficient A_4, which is the coefficient of the fastest decay term, is the most dominant one. However, this does not mean that this event is the one happening most frequently in the ensemble because a very short lifetime of this decay component makes the total number of occurrences of this event very low, making it the weak contributor to the overall photoluminescence. Therefore, the coefficients themselves cannot be representative for the total number of times an event occurred for which the radiative decay rates of the species should also be taken into account [59]. A more accurate way of extracting the spectral distributions of the events is to utilize the integral in Equation 3.2 (integrated TRF terms) instead of just the coefficients alone at all emission photon energies, as explained above. Therefore, the integrated TRF curves depicted in Figure 3.2.2(b) are physically the most meaningful and important. These results presented in Figure 3.2.2(b) look like steady state photoluminescence (SS-PL) measurement results but they cannot be obtained with a steady state method because of the overlapping spectral distributions and hence spectral mixing of the corresponding events.

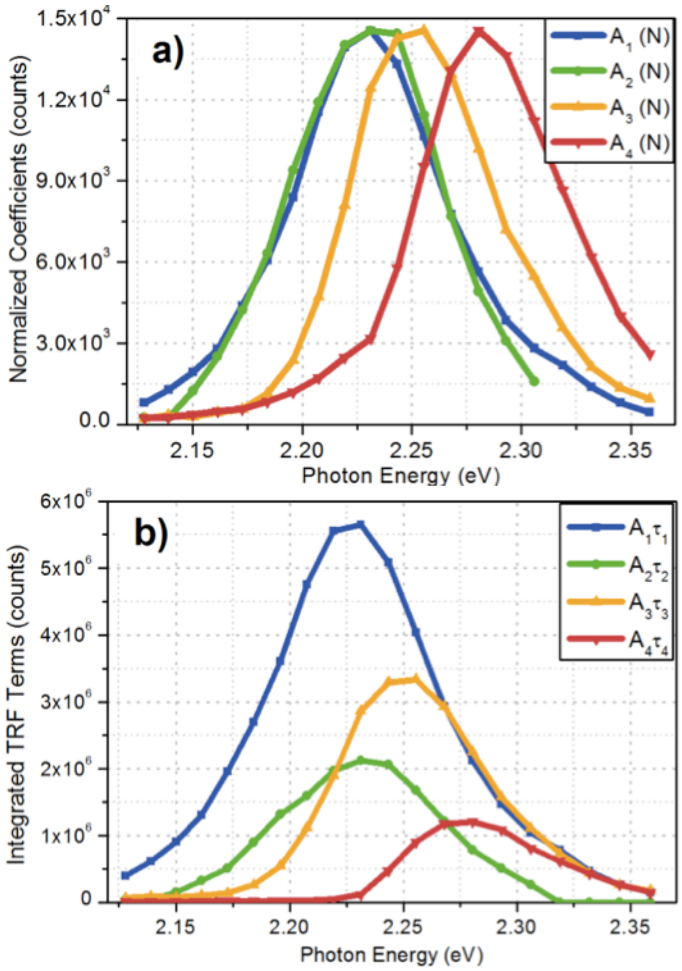

Figure 3.2.2. a) Spectral distributions of normalized TRF fitting coefficients, $A_i(N)$ for event $i=1,2,3,4$. b) Spectral distributions of TRF integrated fitting terms, $A_i\tau_i$ indicating the relative number of events taking place at a photon energy, for event $i=1$, 2, 3, and 4. (Reprinted with permission from Cihan et al. [1] Copyright 2013 American Chemical Society.)

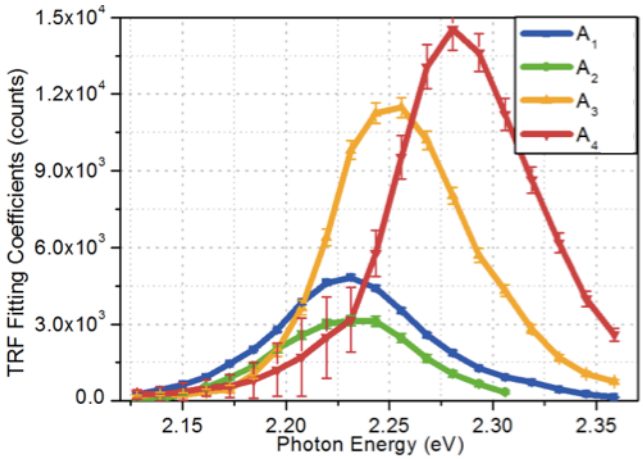

Figure 3.2.3. Spectral distributions of TRF fitting coefficients. (Reprinted with permission from Cihan et al. [1] Copyright 2013 American Chemical Society.)

3.3 Excitation Intensity Dependences of the Integrated TRF Terms

We also obtained the excitation intensity dependences of these events by collecting the spectral distributions of the integrated TRF terms at different excitation intensities. Figure 3.3.1(a) shows the dependences of the spectrally integrated total photon emissions of the corresponding events on the excitation intensity. The intensity dependences of the total number of generated biexcitons (BXs) and trions are directly obtained by the spectral integration of $A_i\tau_i$, i.e., $\int_{510nm}^{580nm} A_i e^{-t/\tau_i}\, d\lambda$ (i = 2 or 3), where $A_i\tau_i$ is the time integral of the decay component $A_i e^{-t/\tau_i}$, i.e., $\int_t A_i e^{-t/\tau_i}\, dt$. In other words, this corresponds to double integral (spectral time integrals) of the decay component. This integral was calculated at each of the excitation power levels and the values were plotted with respect to the excitation intensity. However, the intensity dependence of the total number of single excitons (Xs) generated directly upon a photon absorption is a little bit tricky to calculate because single excitons are generated in QDs also

as a result of a BX recombination. Therefore, the Xs generated due to BX recombination should be excluded. Since each BX recombination event causes a X to be generated and $A_3\tau_3$ is the number of BX recombinations, the number of Xs generated directly from photons is equal to $\int_{510\,nm}^{580\,nm} \left(A_1\tau_1 - A_3\tau_3\right) d\lambda$. The results of this integral at every excitation power level were plotted against the intensity values in Figure 3.3.1(a).

As can be seen in Figure 3.3.1(a), the total number of occurrences of the event that is represented by A_3 and τ_3 exhibits nearly a quadratic excitation intensity dependence while the one represented by A_1 and τ_1 has a linear dependence. These characteristic behaviors are exactly what would be expected from BX and X recombination events, respectively. The linear dependence of X recombination on the excitation intensity is straightforward, which basically comes from a single photon absorption generating a single X to recombine. The nearly quadratic dependence of $A_3\tau_3$ is, on the other hand, due to the cascaded absorptions of two photons within a single pulse by a single QD, which result in the formation of BXs. Therefore, the likelihood of forming a BX quadratically increases with increasing excitation intensity. In fact, this quadratic behavior is considered to be a lucid evidence of the biexcitonic origin of this decay component [35,50,60]. (Here note that there is another component indicated as trions in Figure 3.3.1, which will be examined at a later point in the thesis. Here it is worth noting that this component is growing with the excitation intensity faster than X's and slower than BX's.)

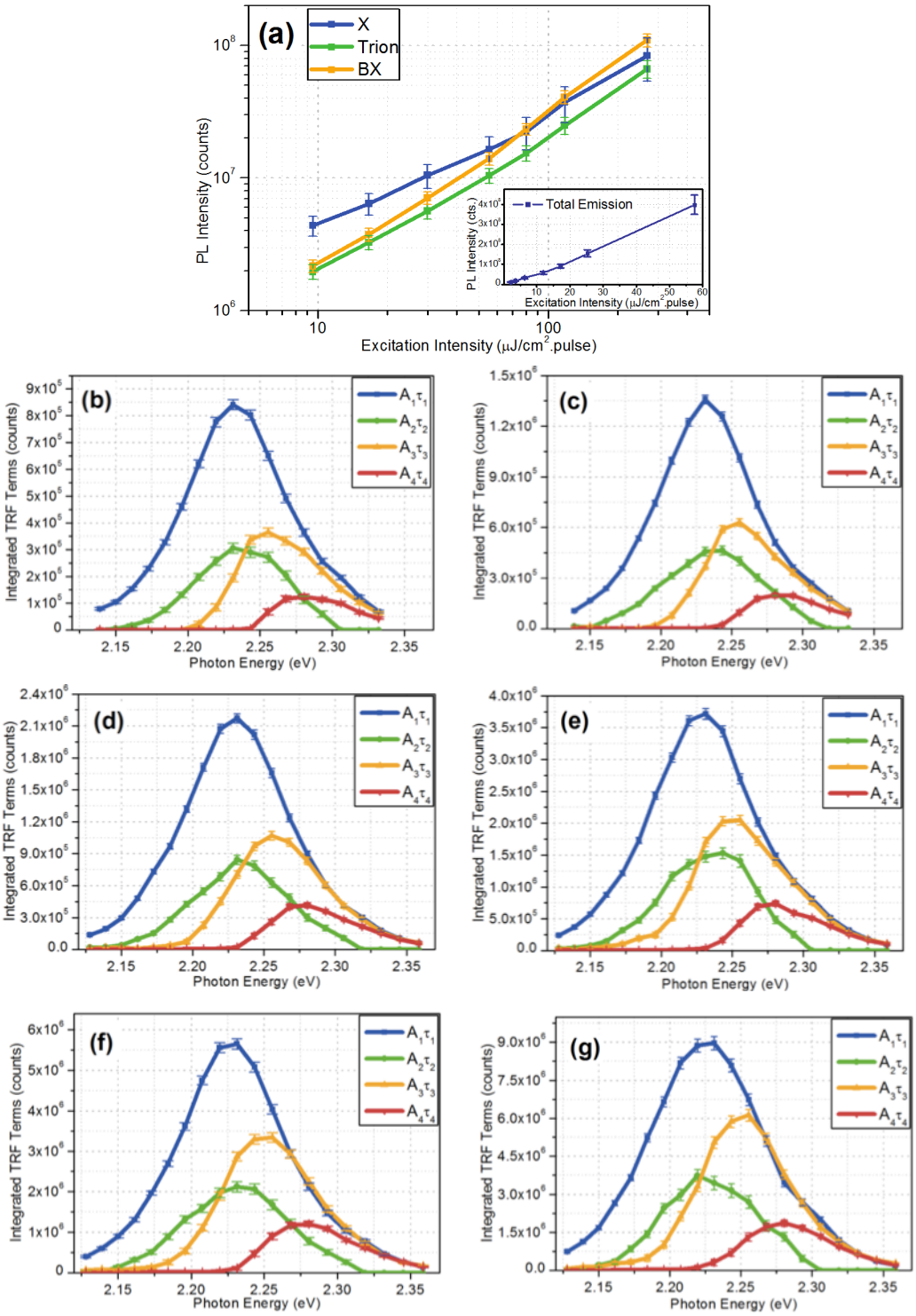
(a)
X
Trion
BX
PL Intensity (counts)
Excitation Intensity (μJ/cm².pulse)
Total Emission
PL Intensity (cts.)
(b)
(c)
(d)
(e)
(f)
(g)
Integrated TRF Terms (counts)
Photon Energy (eV)
A1τ1
A2τ2
A3τ3
A4τ4

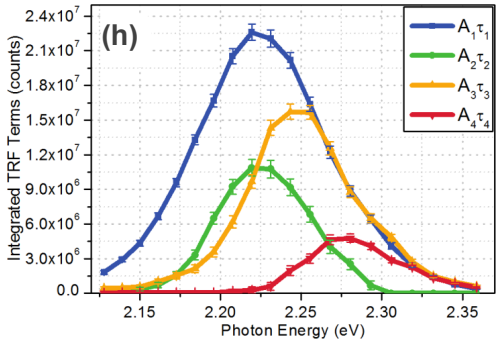

Figure 3.3.1. a) Dependences of the total numbers of X, trion and BX recombination events on the excitation intensity. (inset) Excitation intensity dependence of the total emission from the sample integrated spectrally and in time. b)-h) Spectral distributions of the integrated TRF terms for the excitation pulse intensities: b) 9.5 μJ/cm^2·pulse ($\langle N \rangle$ = 0.05), c) 16.6. μJ/cm^2·pulse ($\langle N \rangle$ = 0.09), d) 29.8 μJ/cm^2·pulse ($\langle N \rangle$ = 0.16), e) 55.5 μJ/cm^2·pulse ($\langle N \rangle$ = 0.29), f) 80.2 μJ/cm^2·pulse ($\langle N \rangle$ = 0.43), g) 117.4 μJ/cm^2·pulse ($\langle N \rangle$ = 0.62), and h) 268.1 μJ/cm^2·pulse ($\langle N \rangle$ = 1.43). (Reprinted with permission from Cihan et al. [1] Copyright 2013 American Chemical Society.)

The spectra of each of the integrated TRF terms at the intensity levels used to construct Figure 3.3.1(a) are provided in Figures 3.3.1(b)-(h). The three plots are scaled without changing the photon counts numbers so that the $A_1\tau_1$ peaks are at the same level in order to guide the eye about the dominance of the integrated TRF terms. As can be seen from Figure 3.3.1(b)-(h), as the excitation intensity increases, the BX recombination becomes more dominant, which is consistent with the trend given in Figure 3.3.1(a). The increased dominance of the coefficient A_3 (see Table 3.2.1) of the TRF decay curve in Figure 3.2.1 with the increased intensity is a result of the same fact that BXs become more dominant with the increased excitation intensity.

The facts that QDs have a near unity QY and experiments were conducted at cryogenic temperatures ensure a high degree of suppression of other

nonradiative and non-ideal transitions caused by the interfacial and surface defects. Therefore, the resulting TCSPC decay curves were expected to consist mostly of radiative recombination terms. As shown in the inset of Figure 3.3.1(a), the total emission from the sample has a linear excitation intensity dependence suggesting that the features generated at higher intensities are also primarily radiative pointing towards a significant suppression of nonradiative Auger recombination.

3.4 Verification of Attributions of Decay Components to the Physical Events via Other Supporting Results

3.4.1 Decay Lifetime Values of TRF Terms

In addition to the quadratic intensity dependence and coherent spectral behavior of the decay term $A_3\tau_3$, the lifetime of this component is also a strong evidence for the biexcitonic origin of this component. Throughout the entire spectrum, for all excitation intensity levels, the lifetime of this component, τ_3, is found to be very close to the $1/4^{th}$ of the single exciton recombination lifetime, τ_1 (See Figure 3.4.1.1). This ratio of BX radiative recombination rate to the X recombination rate is expected to be 4 according to the quadratic scaling of the recombination rates with the exciton multiplicity, which was previously proposed and supported through "free carrier model" by McGuire *et al.* and also by some other reports [6,61]. The reason behind the quadratic scaling of recombination rates is that there are N^2 possible recombination pathways for a QD with N excitons in it, as illustrated in Figure 1. Therefore, the "free carrier model" can be said to hold true for this core/shell material combination both for the giant QDs reported previously [35] and for these QDs reported here. The range of BX recombination lifetime and the clear shift of the photoluminescence spectra with time suggest that the recombination events of BXs through the TRF

fitting term $A_3\tau_3$ are radiative and they take place in the QDs that exhibit AR suppression. Although AR suppression is clearly present in the ensemble, there may be also a sub-ensemble of QDs that does not exhibit AR suppression in our sample as is the case of some previous reports in the literature [34,38,61]. If there exists, the recombination dynamics of BXs generated in QDs without AR suppression, i.e., the nonradiative part of the BX dynamics, is included in the $A_4\tau_4$ term having a sub-nanosecond lifetime, as expected from AR, which will be discussed later in the thesis.

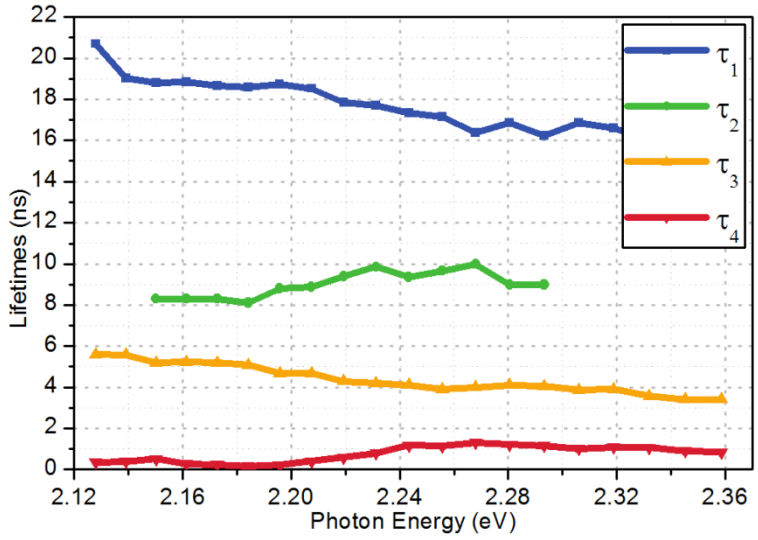

Figure 3.4.1.1. Spectral distributions of the lifetime of each decay term. (Reprinted with permission from Cihan et al. [1] Copyright 2013 American Chemical Society.)

3.4.2 Temporal Evolution of the Photoluminescence Spectrum of QDs

The results of TRF decay measurements throughout the entire spectrum can also be analyzed by looking at the temporal cuts of the decay results at all wavelengths like previously reported in the literature [36,62]. Although the previous approach gives less information about the multiexcitonic behavior of the sample under test compared to the method used in this thesis, the former is

easier to conduct and understand than the latter. Temporal evolution of the emission spectra of the sample after the laser pulse excitation is given in the inset of Figure 3.4.2.1. As can be seen in the figure, the PL spectrum shifts towards longer wavelengths as time passes after the excitation pulse hits the sample. This shift results from the BX emission, which takes place in the blue tail of the X peak and has a shorter lifetime compared to the X emission. Therefore, the emissions from BX states of the QDs diminish before the emissions from X states do and the total emission spectrum shifts to the X emission side over time. For a quantitative analysis, the shift of the PL peak position in time is depicted in Figure 3.4.2.1. If the recombination of the BXs in all of the QDs were totally nonradiative *via* AR process, the time needed for the PL peak to come to the final PL peak position, where the X emission takes place, would take 1-2 ns because of the very short sub-nanosecond lifetime of the AR process. However, it is shown in Figure 3.4.2.1 that it takes more than 20 ns for the PL peak to arrive at the eventual position where emissions are only from the X states of the QDs. These results support the claims that BXs emit at higher photon energies in these QDs and possess a lifetime around 4-5 ns as obtained with the TRF decay fitting results. The long lifetimes of BXs compared to typical AR lifetimes of BXs support that AR is suppressed in a substantial portion of the QDs in the ensemble. This is consistent with the conclusion drawn from the linear intensity dependence of total emission from the sample (inset of Figure 3.3.1(a)).

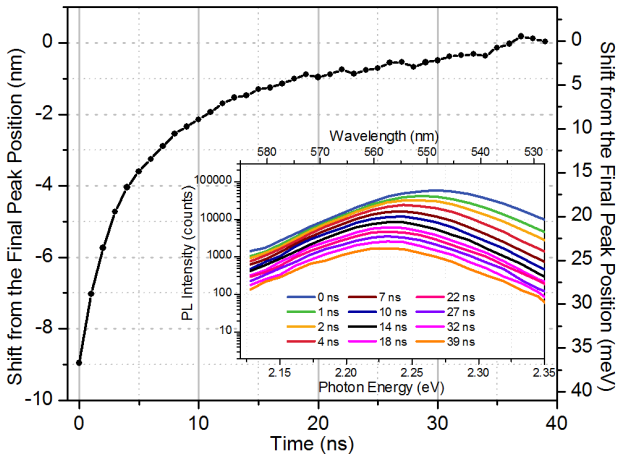

Figure 3.4.2.1. Time dependence of the PL peak position shift with respect to the final position under the excitation fluence of 2.6x10^{14} photons/cm^2 per pulse ($\langle N \rangle$ = 0.74). (inset) Evolution of the PL spectrum with time. (Reprinted with permission from Cihan et al. [1] Copyright 2013 American Chemical Society.)

3.4.3 Comparison of the Spectra of Integrated TRF Terms to Steady-State Photoluminescence Spectrum of QDs

In order to verify our claim that the $A_1\tau_1$ integrated TRF term is due to the emissions of the X states of the QDs, we conducted TRF and SS-PL measurements at room temperature. In Figure 3.4.3.1, the spectral distributions of the integrated TRF terms under the excitation intensity high enough to generate BXs and trions are compared to the SS-PL spectrum of the same sample taken under very low intensity continuous-wave excitation at 442 nm (3 eV). In the SS-PL measurement, we therefore expect only the emissions from the X states of the QDs to contribute. Since we also attribute the TRF decay term represented by $A_1\tau_1$ to the emission of the X states, one would expect a significant overlap of the $A_1\tau_1$ spectral distribution with the SS-PL spectrum. The results show almost a full overlap as expected. The consistency between totally independent TRF and SS-PL measurements in terms of X emission can be considered as a strong evidence of the $A_1\tau_1$ attribution to the X decay.

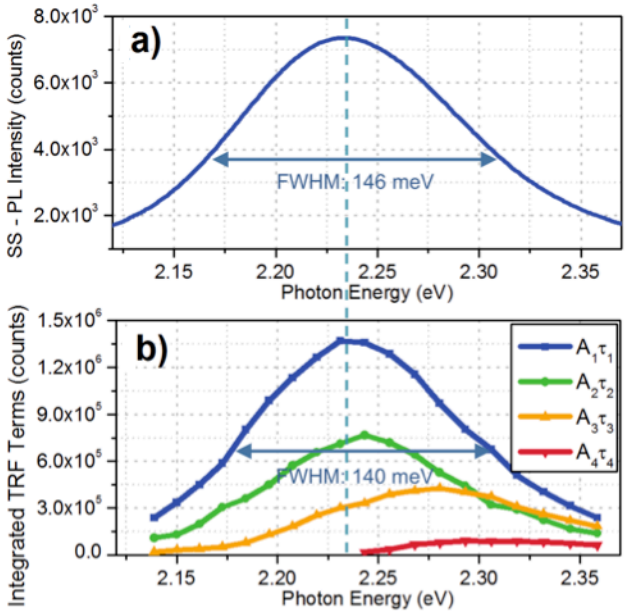

Figure 3.4.3.1. Consistency of spectral behavior of $A_1\tau_1$ term and steady-state PL spectrum. a) The steady-state PL spectrum of the sample. b) Spectral distributions of the integrated TRF decay terms under the excitation fluence of 5.1x10^{14} photons/cm^2 per pulse ($\langle N \rangle$ = 1.43). (Dashed vertical line emphasizes the peak positions of the spectra.) (Reprinted with permission from Cihan et al. [1] Copyright 2013 American Chemical Society.)

3.4.4 Sample Exposure Time Dependences of Integrated TRF Terms

In the previous parts where we discussed the BX and X recombination events, the results for the attribution of $A_1\tau_1$ term to X and $A_3\tau_3$ term to BX recombination events were provided. Figure 3.4.4.1 presents the necessary information for us to make comments on the remaining two components of the overall TRF decay, $A_2\tau_2$ and $A_4\tau_4$.

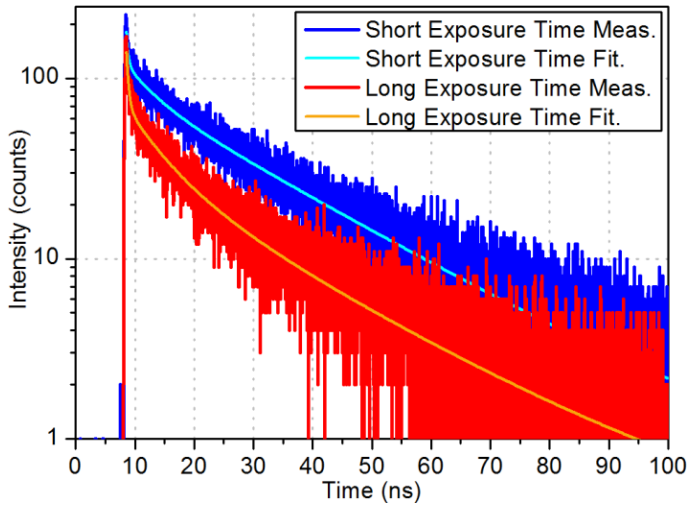

Figure 3.4.4.1. Experimental measurement and corresponding numerical fitting for the TRF decays of the QD sample at the PL emission peak under short and long exposure times to the laser excitation of 5.1×10^{14} photons/cm^2 per pulse ($\langle N \rangle = 1.43$). (Reprinted with permission from Cihan et al. [1] Copyright 2013 American Chemical Society.)

Table 3.4.4.1. Fitting results of short and long exposure time cases plotted in Figure 3.4.4.1.

	A_1	τ_1 (ns)	A_2	τ_2 (ns)	A_3	τ_3 (ns)	A_4	τ_4 (ns)	Total Count	Avg. Lifetime
Short Exp.	82±3	23.2	-	-	36±12	4.81	63±54	0.323	1.52×10^5	11.59 ns
Long Exp.	26±2	23.7	14±5	11.09	31±7	5.08	71±36	0.381	7.26×10^4	6.77 ns

Figure 3.4.4.1 shows two TRF decays of the QD solid sample under exactly the same excitation conditions for the same data collection duration only using different times of exposure to the laser beam. The blue curve is the case when the sample is exposed to the light for a few seconds whereas the red one is the decay curve of the sample after an exposure to the laser beam for 15 min. The corresponding fitting parameters are given in Table 3.4.4.1. For this experiment, we expect the radiative and nonradiative recombination events of charged QDs to become more dominant for the case of longer exposure time because of the accumulation of the charged QDs in the ensemble. Especially, the radiative and nonradiative decay terms of trions from the QDs with and without AR

suppression, respectively, are expected to dominate. As can be seen from Figure 3.4.4.1 and Table 3.4.4.1, for the longer exposure time case, the total emission of the QDs decreases considerably because of the increased amount of nonradiative AR, which is enhanced due to the photocharging of the QDs. Since it is well established that the typical AR lifetimes for this kind of QDs are on the order of 100s of ps, we expect to have a more pronounced coefficient of the decay term with a lifetime of 300-400 ps, which is A_4. The increase of A_4 coefficient with the exposure time, as shown in Table 3.4.4.1, means that at least a good portion of the 300-400 ps lifetime component is due to the AR of trions. (Despite the fact that the experimental time resolution is not high enough to obtain exact lifetimes and coefficients of AR, we could still obtain conclusive results and make qualitative comments about the dominancy of the corresponding decay component.) In addition to the nonradiative AR of trions, we observe an increase in the coefficient A_2, which we believe is the coefficient related to the radiative recombination of trions in the QDs with suppressed AR behavior. The trions with radiative recombination behavior are believed to be negatively charged ones because the AR probability for positively charged trions is higher due to the high degree of spatial confinement for holes in this material system [63]. The lifetime value, τ_2, is ca. $1/2^{nd}$ of the lifetime of the X decay, τ_1. This is another supporting result for the claim that $A_2\tau_2$ corresponds to the radiative decay of trions consistent with the free carrier model [6] and other reports in the literature [64]. The observation of radiative recombinations of trions from the ensemble is considered to be a good sign of substantially suppressed AR [49]. Also, in Figure 3.3.1(a), it is observed that the total number of occurrences of trion recombinations represented by the spectral integration of $A_2\tau_2$ exhibits a sub-quadratic and super-linear dependency on the excitation intensity, which is yet another supporting evidence for the observation of trions.

3.4.5 The Decay Term Attributed to the Nonradiative Processes

The last decay term that was observed in the TRF measurements is the $A_4\tau_4$ decay term that we attribute to the nonradiative recombinations of trions, BXs, charged BXs, and species of higher multiplicity that are generated in the QDs without AR suppression whereas the first three decay terms were purely radiative. In our study, we do not observe a significant radiative recombination from the charged BX states in the QD ensemble. This could be due to the higher dominancy of AR in accordance with the very strong positive dependence of AR rate on the charge carrier number in the QDs, which makes the radiative recombination from charged BX states less likely. When the temperature was decreased to cryogenic temperatures, we observed that the $A_4\tau_4$ decay term became more pronounced at all emission photon energies. This shows that, in addition to the nonradiative AR of BXs and trions, the $A_4\tau_4$ decay term has some contribution from the emission of the singlet states before the system comes to the thermal equilibrium between the singlet and triplet states [65], [66]. Further details of this very fast component were not investigated in this study and are out of the scope of this thesis work. However, with a higher time resolution characterization, the spectral and temporal behavior of these very fast events could also in principle be resolved with the systematic method employed here. The important point regarding this very fast weak component for our work here is that this component does not affect the results we obtained and conclusions we drew about the other terms of the overall decay.

3.5 Quantum Dot Core Size Dependences of the Spectral Behaviors of Biexcitons, Trions and Single Exciton

Besides the QDs whose spectral X, trion and BX behaviors are provided in Figure 3.3.1, we measured and obtained integrated TRF decay terms under high intensity excitation for two more CdSe/CdS QDs, one with a smaller core size and one with a larger core size, while both using the same shell thicknesses as the previous middle-sized QD sample. As can be seen in Figure 3.5.1(a), the spectra for the QDs with the largest core, the BX peak is almost at the same spectral position as the X peak. The BX-X peak shift is 30 meV and 43 meV for the middle-sized (Figure 3.5.1(b)) and the smallest core (Figure 3.5.1(c)) QDs, respectively. The reason for the trend of the higher energy BX formation compared to the Xs for the smaller-core QDs is that the delocalization of the electrons over the shell region of the QDs increases with decreasing the core radius, which results in a more Type-II-like behavior. For the large core case provided in Figure 3.5.1(a), the local charge neutrality in the QDs is not sufficiently distorted to observe a repulsive X-X interaction and, hence, a blue-shifting BX with respect to the Xs is not observed. The relative spectral tunability of BXs with respect to Xs is a feature that makes the material system of CdSe/CdS much more promising compared to the other core/shell QD material systems, such as CdSe/ZnS. This feature will be discussed in more detail in the upcoming chapters of the thesis.

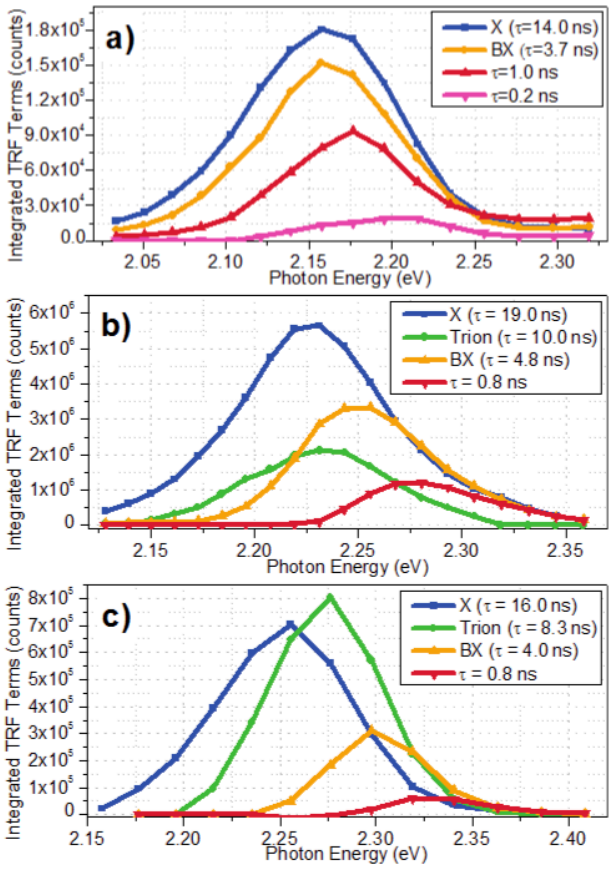

Figure 3.5.1. Spectral behavior of the integrated TRF terms of three different size QDs with the core radii of *ca.* a) 1.80 nm, b) 1.22 nm and c) 1.10 nm. The shell thicknesses of the QDs are *ca.* 1.4 nm. The excitation fluences for all the cases are 5.1x10^{14} photons/cm^2 per pulse. (Reprinted with permission from Cihan et al. [1] Copyright 2013 American Chemical Society.)

Chapter 4

Exciton-Exciton Interaction Engineering and Amplified Spontaneous Emission of CdSe/CdS Nanocrystals

As mentioned previously, the bandgap tunability of QDs is a very important feature of QDs for lasing and optical gain applications because the conventionally used optical gain media works only at the wavelength of the optical atomic transition of the material. Therefore, if QDs can be used as optical active gain media for lasers, it will be possible and very simple to obtain lasers at all wavelengths that would open a lot of new application areas for lasers. Towards this goal, researchers have recently put a significant amount of effort on the QD lasing and optical gain studies [20,21,67–70].

4.1 CdSe/CdS Quantum Dots

Owing to their size tunable and favorable optical properties, semiconductor colloidal QDs have become highly attractive as light generating materials for light-emitting diodes [71–73] and as optical gain media for lasing applications [20]. Strong quantum confinement effects observed in QDs lead to several advantages over their bulk-counterparts including enhanced exciton binding energies and efficient band edge emission at room temperature due to the increased charge carrier concentration in small QD volumes. QDs also allow for engineering of their electronic fine-structure via tuning of their size [72], shape (spherical, nanorod-shaped [74] and tetrapod-shaped [75]) and excitonic characteristics resulting in distinct electronic behavior; namely, Type-I, Type-II [21] or quasi-Type-II. Consequently, QDs have arisen as a promising class of lasing materials offering lower optical gain thresholds, higher temperature insensitivity, ease of processability via facile wet-chemistry methods, and ease of emission tunability covering a wide specral range. These attributes make QDs appealing as compared to other emerging material systems including organics and epitaxially templated quantum-confined systems.

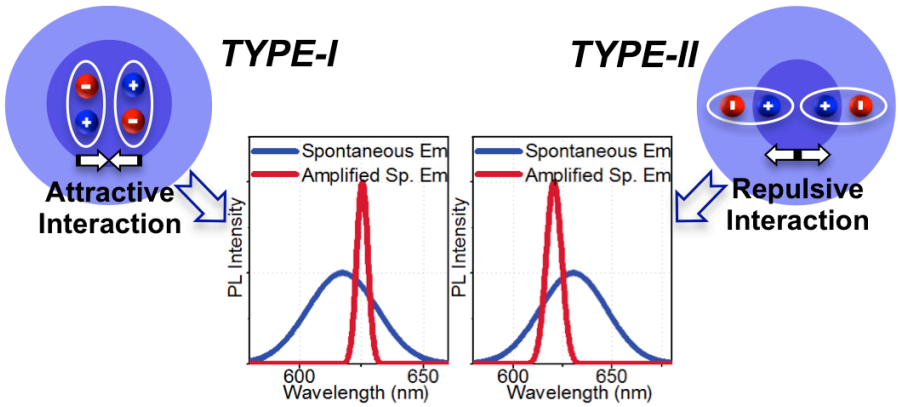

Figure 4.1.1. The electron/hole localization and the corresponding spectral amplified spontaneous emission and spontaneous emission behaviors.

Optical gain performance of various QDs has previously been studied and relatively low optical gain thresholds have been reported with respectable temperature stabilities and narrow emission bandwidths [19]. Optically pumped QD lasers have been realized using various photonic structures (e.g., in optical cavities made up of distributed Bragg reflectors, above grating structures providing distributed feedback) [22,76–78]. In these previous studies, single-photon absorption mechanism was utilized for optical pumping. Also, in few recent studies, as an alternative to single-photon optical pumping, TPA mechanism [79–82] was employed to realize ASE in QDs, which offers a lower risk of photo-damaging the sample. This is also advantageous because QDs exhibit very high TPA cross-sections [83-85]. Among these previously studied QD systems are CdSe/CdS/ZnS core/shell/shell QDs [79–82] and CdSe/CdS nanorods [86].

As a unique and fundamental feature of core/shell and multi-shell QDs, the core-shell size adjustments provide us with the ability to control the nature and strength of exciton-exciton (X-X) interactions by tuning electron and hole wavefunction localizations across the core and the shell [87]. Therefore, the repulsive (Type-II-like) vs. attractive (Type-I-like) nature of X-X interactions can be engineered to modify optical and electronic properties [88–90]. Within this context, Cooney et al. has recently shown tunable ASE from s and p states of the QDs via state-resolved pumping [91], but the potential of the electronic-type engineering of the QDs for lasing applications was not considered. In the work of Saba et al., in seeded CdSe/CdS core/shell nanorods, tuning of biexciton emission was demonstrated by shifting the electronic structure from Type-I to quasi-Type-II [92]. Although, in principle, quasi-Type-II QDs offer the potential to operate in both regimes [41], to date, no single material system has been shown to exhibit ASE tunability from Type-I-like to Type-II-like behavior, i.e., red- to blue-shifted ASE with respect to spontaneous emission, respectively.

This implies that it should be in fact possible, with the right QD core-shell design, to achieve also non-shifting ASE, which has not been previously achieved. Mastering X-X interactions and developing full control over the ASE are important for performance improvements of QD lasing systems by enabling the engineering and optimization of gain/loss mechanisms in these systems.

In this part of the thesis, utilizing quasi-Type-II CdSe/CdS core/shell QDs and studying their ASE systematically under two-photon excitation, we present the absolute and relative tuning of the ASE characteristics going from Type-I-like to Type-II-like regimes in a single material system, as pictorially illustrated in Figures 4.1.1 and 4.1.2. These QDs are particularly chosen for this study, as they offer near-unity QY with significantly suppressed Auger recombination, as a result of the partial separation of electron and hole wavefunctions within the core-shell structure [19,38,61,93].

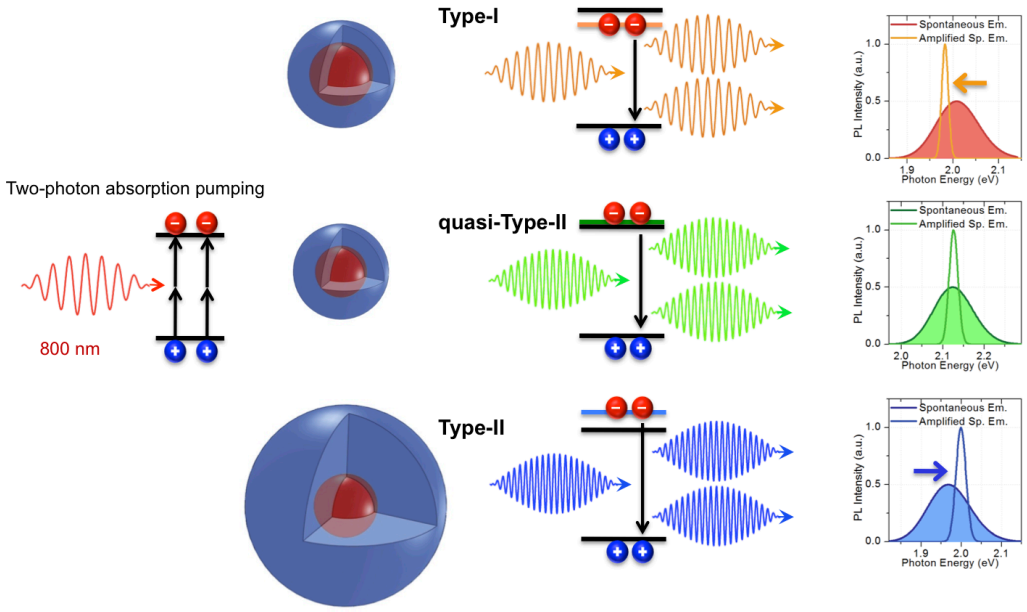

Figure 4.1.2. Schematics of the TPA-pumping of quasi-Type-II CdSe/CdS core/shell QDs and relative tuning of their ASE *via* Type-tuning of these QDs by core/shell dimension

adjustments resulting in red- to blue-shifted ASE peak with respect to spontaneous emission. Also, here note the non-shifting ASE between the red- and blue-shifting regimes.

As will be shown in the next subsection, the TPA cross-section of these QDs, measured by z-scan technique at 800 nm excitation wavelength, was found to be ca. 44660 GM, which is one of the highest reported values when compared to the QDs of similar size. This resulted in the observation of a very low optical gain threshold value of 6.5 mJ/cm^2 per pulse at 800 nm excitation wavelength without any loss compensation or waveguiding mechanism. Using these CdSe/CdS QDs, the tunability of the ASE peak with respect to spontaneous emission was achieved via carefully engineering their X-X interactions by changing the core size and shell thickness of the QDs. Here we showed that a single material system can exhibit full ASE tuning variation from blue- to red-shifting behavior, and non-shifting ASE is possible between these two regimes. The ASE peak shift we obtained for CdSe/CdS QDs in the blue-shifting regime is 32 meV (about 10 nm), while it is ca. 25 meV (about 8 nm) in the red-shifting regime. Also, as we will present in the following sections, we demonstrated that there is no unique core-shell combination to obtain certain ASE characteristics and that it is possible to obtain ASE at a specific wavelength of choice within the feasible range both from Type-I-like and Type-II-like excitonically engineered CdSe/CdS QDs.

4.1.1 Two-Photon Absorption Cross-Section Measurement via Z-Scan Technique

Obtaining high TPA cross-section is very critical for achieving low threshold TPA-based optical gain because of the direct correlation between the TPA cross-section and the number of absorbed photons, which determines the onset of population inversion. Although CdSe/ZnS core/shell QDs are the most

commonly employed QDs in optical gain studies, their lower TPA cross-sections compared to that of CdSe/CdS core/shell QDs make them unfavorable against CdSe/CdS QDs for TPA-based optical gain studies. Therefore, in order to verify the high TPA cross-section values of CdSe/CdS QDs, we conducted open-aperture *z*-scan measurements of CdSe/CdS QDs having a core diameter of 3.2 nm and a shell thickness of 1.1 nm. The transmission result and the corresponding fitting curve are given in Figure 4.1.1.1. The measurement was taken under the same pumping source that was used for the ASE measurements. The transmission result was fitted with Equation 4.1,

$$T(z) = \frac{1}{1 + \frac{I_0 \times \beta \times l}{1 + (z/z_0)^2}} \tag{4.1}$$

where I_0 is the peak intensity at the focus of the excitation, β is the two-photon absorption coefficient, l is the optical path-length of the sample, and z_0 is the Rayleigh range [84]. The experimental transmission result was fitted with the best fitting parameter of TPA coefficient of $\beta = 5.96\times10^{-15}$ m/W. Substituting this value into Equation 4.2,

$$\sigma_2 = \frac{h \times \nu \times \beta}{N_A \times d_0 \times 10^{-3}} \tag{4.2}$$

where $h\nu$ is the photon energy, N_A is the Avogadro's number, and d_0 is the molar concentration of the QDs in solution [84] .This analysis resulted in a TPA cross-section value of $\sigma_2 = 44660\ GM$, which is a very high TPA cross-section value for CdSe/CdS QDs compared to organic dyes and CdSe/ZnS QDs of similar sizes and suggests that CdSe/CdS QDs are very strong two-photon sensitizers. The higher TPA cross-section of CdSe/CdS QDs can be explained by the fact that the lower band gap value of CdS (2.5 eV) compared to that of ZnS (3.9 eV) [94] causes more absorption in the shell region of the QDs to occur; hence, TPA

cross-section in of CdSe/CdS structure is higher compared to that of CdSe/ZnS structure.

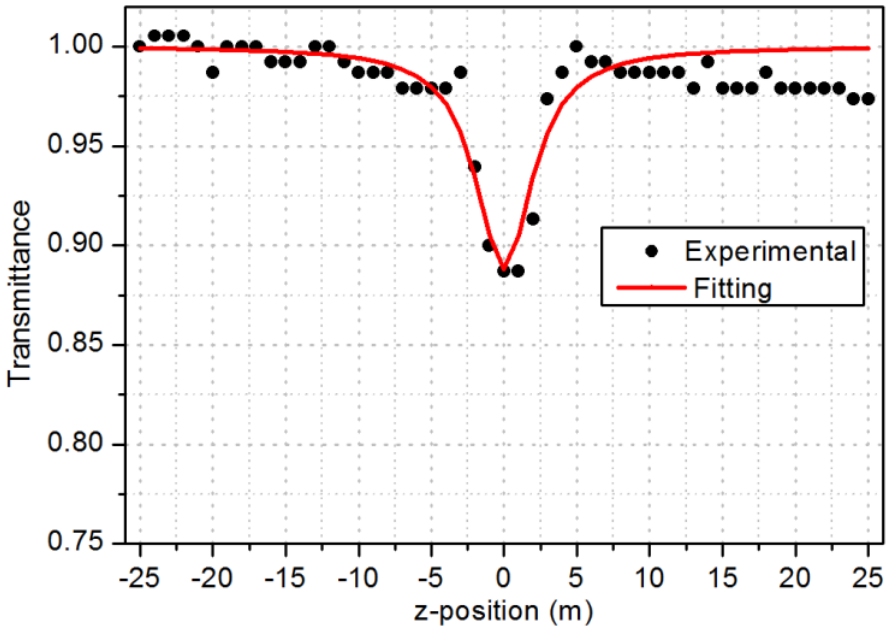

Figure 4.1.1.1. Transmittance result of the open-aperture Z-Scan experiment and the fitting of the result using Equation 4.1. We found the TPA cross-section value to be $\sigma_2 = 44660\ GM$, which is very high compared to CdSe/ZnS QDs of similar sizes [79]**. Hence, CdSe/CdS QDs stand out as promising two-photon sensitizers. This higher TPA cross-section of CdSe/CdS QDs compared to CdSe/ZnS can be explained by increased contribution coming from the CdS shell having a band gap of 2.5 eV (see Figure 3.1.1.2 for the absorption of CdSe/CdS QDs exhibiting a strong kink around 430 nm due to the absorption of the CdS shell) while the ZnS shell has a too large band gap (3.9 eV) that it cannot contribute to the TPA at 800 nm (1.55 eV)** [94]**.**

4.1.2 Amplified Spontaneous Emission Experiments of CdSe/CdS Quantum Dots

4.1.2.1 Sample Preparation and Steady-State Photoluminescence Experiment Setup

The thin-film samples of QDs were prepared by drop-casting highly concentrated (ca. 50 mg/ml) solutions of QDs dissolved in hexane on 1 cm by 1 cm quartz substrates. Then the solvent was allowed to slowly evaporate at room temperature leaving very highly stacked QD layers on top of the quartz substrates.

For ASE experiments, as the excitation source for the QD samples, we used femtosecond optical amplifier (Spectra Physics, Spitfire Pro XP) with an output beam of a 45 fs pulse width at 800 nm wavelength. The amplifier is seeded by a Ti:Sapphire laser (Spectra Physics, Tsunami). The laser beam is focused to a spot whose area is ca. 1 mm^2 on the sample with the help of a thin lens with a 10 cm focal length. The emission spectra of the samples were collected by an optical fiber connected to a miniature spectrometer (Ocean Optics).

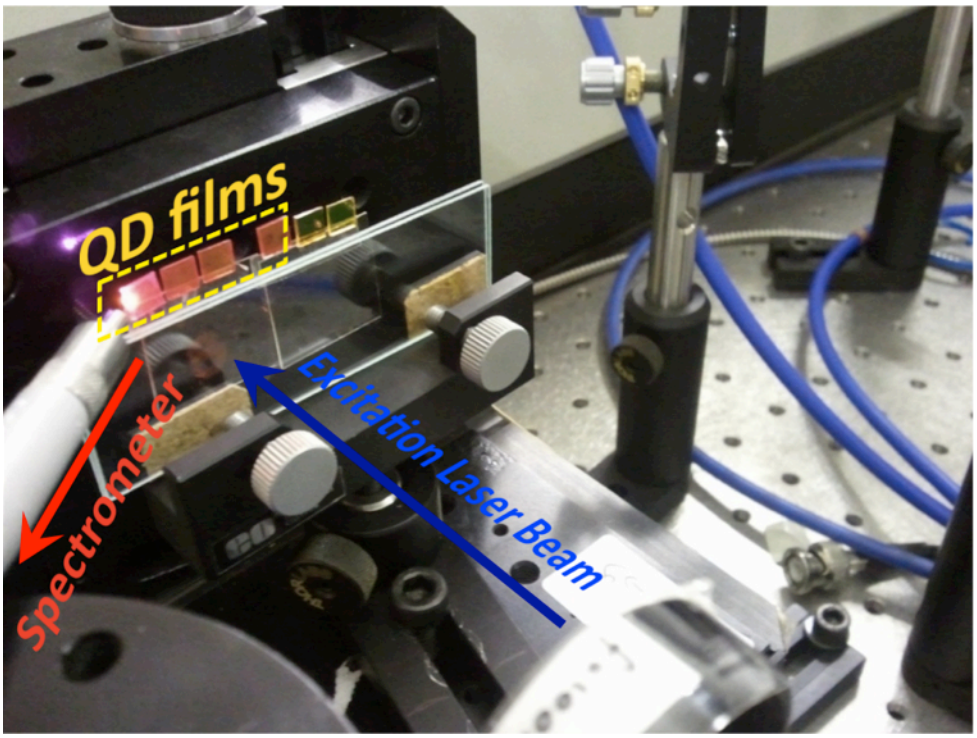

Figure 4.1.2.1.1. The steady-state photoluminescence experiment setup and the samples.

4.1.2.2 Experimental Amplified Spontaneous Emission Results and Discussion

ASE performance of highly concentrated drop-casted solid films of CdSe/CdS QDs was investigated through excitation intensity dependent PL emission measurements, as shown in Figure 4.1.2.2.1(a). As can be seen here, when the excitation intensity exceeded the optical gain threshold, ASE peak emerged at a wavelength *ca.* 3 nm (11 meV) longer than of the spontaneous emission peak. The full width at half maximum (FWHM) of the ASE and the spontaneous emission peaks of the sample excited with an intensity of 10 mJ/cm^2 per pulse were obtained as 5.7 and 21.4 nm (19 and 73 meV), respectively, by fitting the PL spectrum with two Gaussian functions. The spectral integration of these two Gaussian functions indicated that, although it is spectrally very narrow, the

emission due to the ASE process accounted for more than 50% of all the emission from the sample in the direction of collection. As shown in Figure 4.1.2.2.1(b), the excitation intensity threshold for ASE is ca. 6.5 mJ/cm^2 per pulse. The ASE performance of this sample can be said to be very good considering the fact that there is no loss compensation or wave-guiding effect favoring the optical gain in the sample. The concomitant spontaneous emission is due to scattering and diffusion of the excitation light, resulting in out-of-focus excitation of the sample.

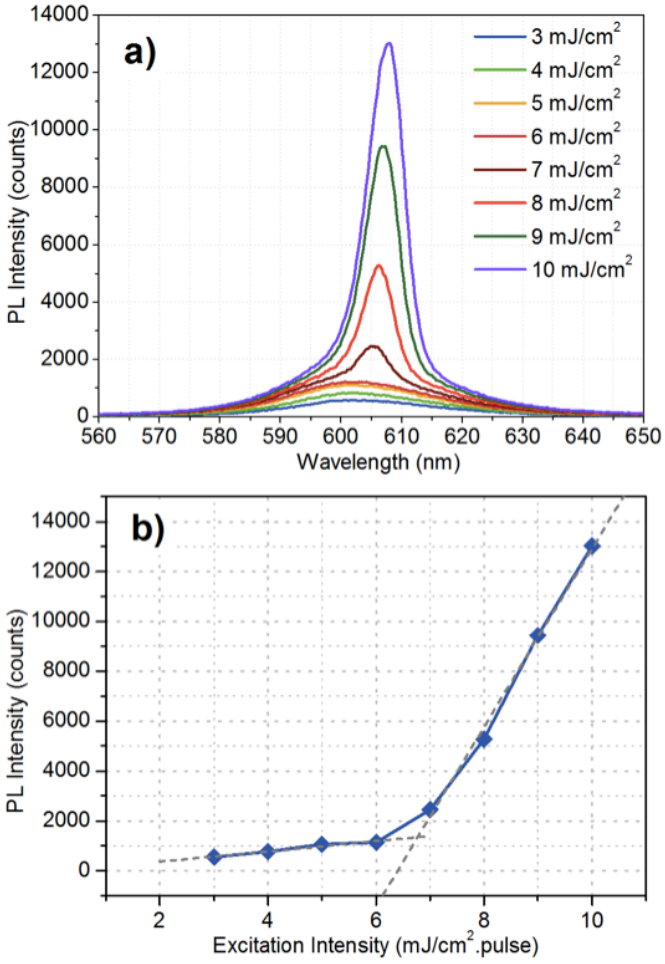

Figure 4.1.2.2.1. a) Evolution of the PL spectra of CdSe/CdS QDs with varying excitation intensity. b) Excitation pulse intensity dependence of the PL intensity at the wavelength of ASE process. The linear fits shown as dashed lines are guides to the eye about the slopes of the curves.

In terms of spectral behavior of the ASE process as depicted above, 3 nm red-shifted ASE was observed with respect to spontaneous emission, whereas this spectral difference is expected to be around 15-20 nm in regular Type-I QDs [79]. This shows that the structure is in the quasi-Type-II regime but it is closer to being Type-I-like rather than being Type-II-like. In other words, 3 nm shift implies that the local charge neutrality is distorted in these QDs as observed in Type-II structures [95]; however, the distortion is not strong enough to give rise to a significant repulsive X-X interaction in the QDs.

4.1.2.3. Demonstration of Type-Tunability Feature of CdSe/CdS Quantum Dots in Their Amplified Spontaneous Emission Spectra

Since ASE occurs from BX states in the QDs used in this study at the reported excitation levels, the spectral positions of BXs and Xs correspond to the spectral positions of the ASE and the spontaneous emission, respectively. Therefore, we successfully tuned the spectral position of ASE by tuning the BX energy via core/shell size adjustments.

To experimentally demonstrate the Type-tunability feature of the CdSe/CdS QDs from Type-I-like to Type-II-like behaviors, three different CdSe/CdS core/shell QDs having different core diameters and shell thicknesses were synthesized. The core/shell sizes of these samples were chosen to obtain repulsive, attractive, and neither repulsive nor attractive X-X interactions corresponding to Type-II, Type-I and quasi-Type-II regimes, respectively. The room temperature normalized PL spectra of the three CdSe/CdS QDs, whose size information is provided in Figure 4.1.2.3.1(b)-(c), under intense two-photon optical excitation are given in the inset of Figure 4.1.2.3.1(a) as a demonstration of relative tunability of ASE. (Note that the QDs whose PL spectra are provided in this figure do not necessarily have near-unity QY since it is not possible to

obtain near-unity QY for all QD sizes. Near-unity QY QDs used in the ASE performance evaluation experiments were discussed previously.) The spontaneous emission and the ASE contributions in the total PL emissions of these samples were extracted by fitting the PL spectra with two Gaussian distribution functions and provided in Figure 4.1.2.3.1(a). The ASE peak is clearly blue-shifted compared to the spontaneous emission peak in QD_3 sample (red curve) while it is red-shifted for QD_2 sample (green curve). However, the ASE peak is almost at the same position as the spontaneous emission of QD_1 sample (blue curve). The reason for the blue-shifted ASE peak in QD_3 is that these QDs have a very thick shell, which allows the electrons to delocalize freely over the entire QD volume while the holes are confined in the core, which results in Type-II-like carrier distributions in these QDs. It is shown in the literature that because of the repulsive X-X Coulomb interactions in Type-II QDs, the BX recombination event takes place at higher photon energies [96]. Since the ASE process occurs from BX states in these samples, as schematically shown in Figures 4.1.1 and 4.1.2, it is blue-shifted in QD_3 sample. On the other hand, the situation is reversed in QD_2 sample where the core is big enough to accommodate both electrons and holes resulting in Type-I-like carrier distributions, and hence an attractive X-X interaction. From the peak overlap of ASE and spontaneous emission events in QD_1 sample, we can say that the carrier distributions in these QDs exhibit a quasi-Type-II behavior, which is the transition regime between Type-I and Type-II. Therefore, the ASE peak is neither blue- nor red-shifted in QD_1 sample.

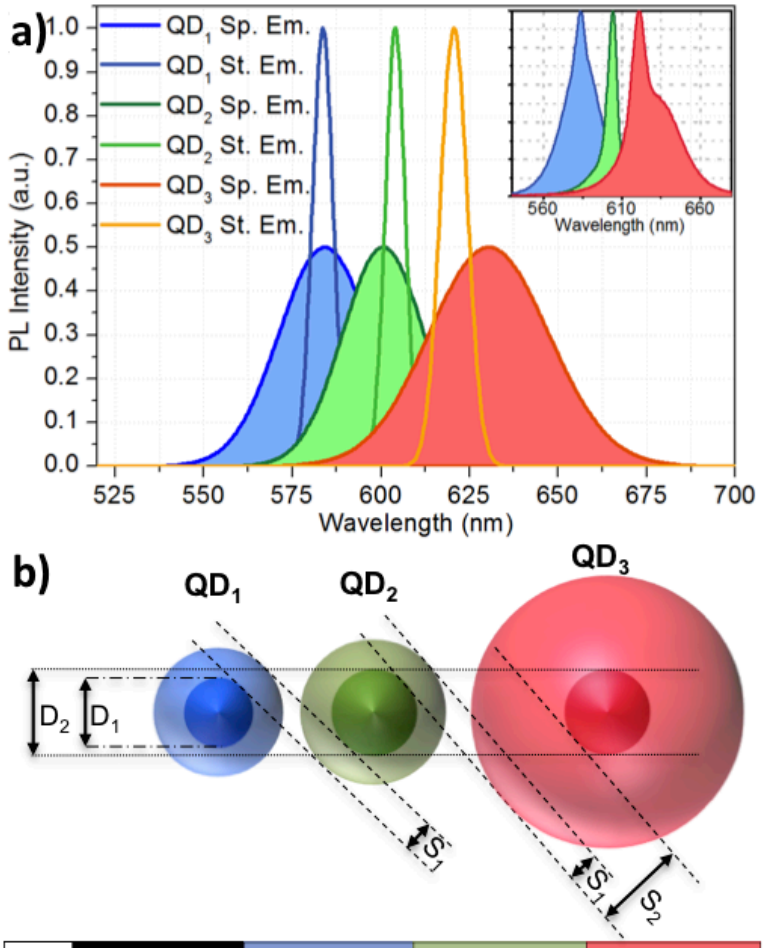

c)	QD_1	QD_2	QD_3
Core Diameter	D_1=2.6 nm	D_2=3.2 nm	D_2=3.2 nm
Shell Thickness	S_1=1.1 nm	S_1=1.1 nm	S_2=3.5 nm

Figure 4.1.2.3.1. a) Normalized decomposed ASE and spontaneous emission spectra of three different QDs under intense two-photon excitation conditions. The under-filled spectra, which are normalized to 0.5 a.u., are the spontaneous emission spectra of the QDs while the narrow spectra normalized to 1 are the ASE spectra of the QDs. The inset shows the original experimental PL spectra of QDs without decomposition. b) Schematics of QDs where the dimensions are proportional to their real dimensions. Dashed lines are provided to compare the core diameters and shell thicknesses of the QDs. c) Table lists the core diameters and shell thicknesses of QDs whose experimental emission spectra are given in a). Note that QD_1 and QD_2 have the same shell thicknesses while QD_2 and QD_3 have the same core radius.

The numerically calculated electron and hole wavefunctions for the two QD sizes of QD_1 and QD_3 samples exhibiting quasi Type-II and Type-II behaviors, respectively, are presented in Figure 4.1.2.3.2. The clear delocalization difference of electrons for these two QD samples is a very good example of the Type-tunability feature of CdSe/CdS QDs.

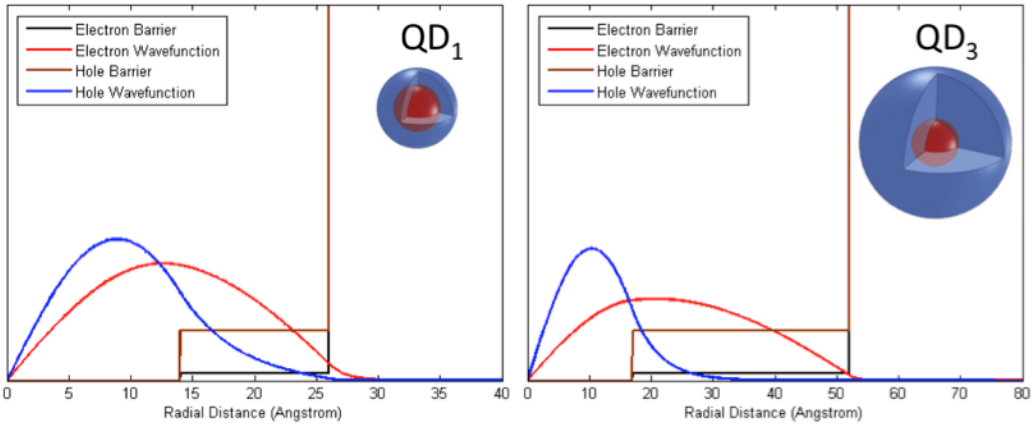

Figure 4.1.2.3.2. Calculated wavefunctions of electrons and holes for QD_1 (on the left) and QD_3 (on the right) samples whose proportionally scaled schematics are provided in the plots.

The physical origin of the relative tunability of spectral position of ASE peak with respect to spontaneous emission peak for this material system is the low energy barrier of 0.3 eV for electrons at the core/shell interface in CdSe/CdS QDs. Because of this low energy barrier for electrons, it is difficult to totally confine the electrons in the core, while the holes are more strongly confined in the core thanks to their larger effective mass and higher energy barrier of 0.78 eV [97]. The only way of confining the electrons in the core is making the core big enough and the shell thin enough as it is the case for QD_2 sample. Being able to adjust the overlap of electron and hole wave functions means that QDs can be made Type-I-like (where both electrons and holes are mostly confined in the same part of the structure) or Type-II-like (where electrons and holes are

confined to different parts of the structure). Therefore, the ASE peak can be manipulated through controlling the BX energies, which have intrinsically opposite signs for Type-I and Type–II systems such that the ASE peak can be chosen to be either on the red or blue side of the PL peak of the QDs [60]. This can provide us with the opportunity to optimize the efficiency of stimulated emission in QDs by deciding whether the optical gain would occur from single exciton states or BX states [21]. Furthermore, the relative adjustability of ASE peak position can enable us to suppress the loss mechanism of re-absorption of the photons that are supposed to contribute to the optical gain process [96].

To verify the claim that one can obtain either Type-I-like or Type-II-like ASE behavior at a specific wavelength from CdSe/CdS QDs by means of this kind of X-X interaction engineering, we conducted ASE experiment on another near-unity QE QD sample whose PL spectra under high intensity pumping is shown in Figure 4.1.2.3.3(a) together with the spectra of QD_3 sample in Figure 4.1.2.3.3.(b) for comparison. As can be seen there, ASE peaks of the samples arise almost at the same spectral position although their spontaneous emission peaks are on the red and blue side of their ASE peaks. This result shows that it is possible to obtain blue- or red-shifted ASE behavior at a specific spectral position from these QDs, which would be a crucial tool for the QD-based single or multi-colour lasing applications.

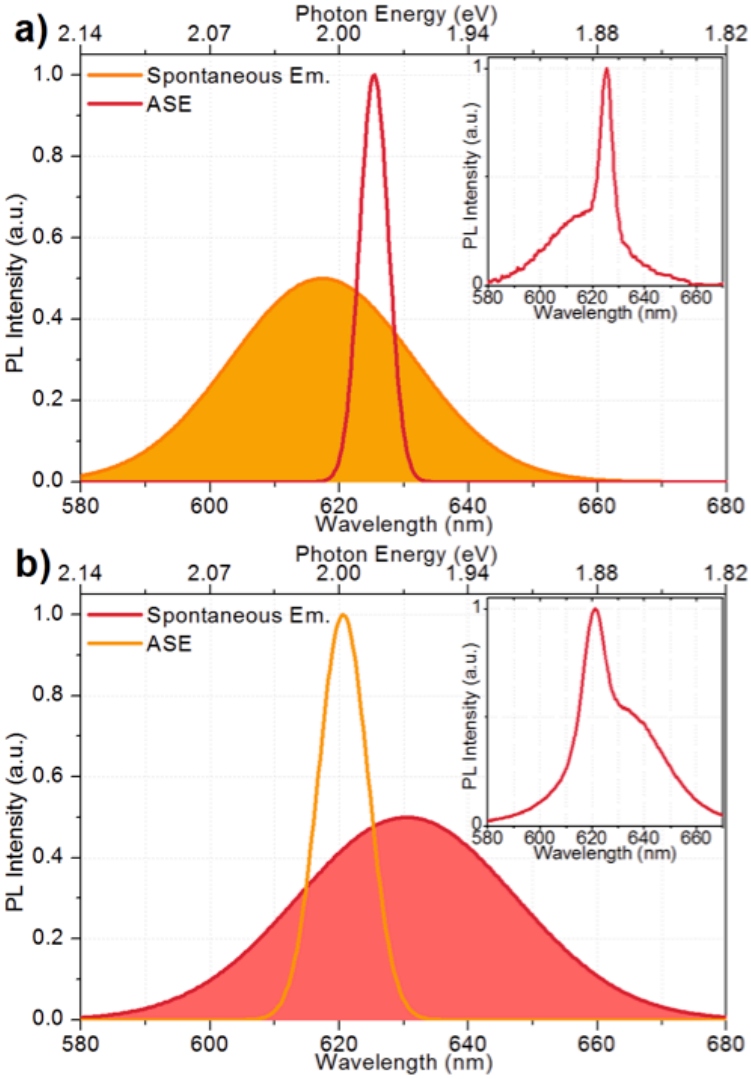

Figure 4.1.2.3.3. Normalized decomposed experimental ASE and spontaneous emission spectra of (a) near-unity QE QDs and (b) QD_3 sample under intense two-photon excitation conditions. The under-filled spectra, which are normalized to 0.5 a.u., are the spontaneous emission spectra of the QDs while the narrow spectra normalized to 1 are the ASE spectra of the QDs. The insets show the original experimental PL spectra of QDs without decomposition.

4.2 CdSe/CdS Nanorods

As a subclass of nanocrystals, core/shell nanorods (NRs) have been extensively considered for nonlinear optics applications and optical gain studies due to the possibility of engineering their electronic structure, longer gain lifetimes and independent absorption-emission tunabilities [92,98,99]. As discussed in the previous chapters about CdSe/CdS material system, with small lattice mismatch resulting in very high crystal quality, very high single- and multi-photon absorption cross-sections and quasi Type-II electronic structure leading to Auger recombination suppression, CdSe/CdS NRs have also become one of the most appealing material systems for lasing applications [34,37,19,100]. The advantage of electron and hole wavefunction overlap tunability feature of CdSe/CdS QDs also exists for CdSe/CdS NRs [74,88,97,101–103]. In other words, it is possible to make CdSe/CdS NRs Type-I or Type-II with size adjustments, which, aside from being of fundamental interest, may be an important design consideration when engineering the gain/loss mechanisms in practical lasing systems [60,89,104]. Furthermore, considering the facts that CdSe/CdS NRs have very high TPA cross-section compared to nanocrystals with different material combinations and two-photon excitation mechanism offers a lower risk of photodamaging the sample compared to conventional single-photon excitation, CdSe/CdS NRs can be said to be one of the most promising optical gain medium candidates [86], [98]. Because of the aforementioned promises, in the nanocrystal lasing context, CdSe/CdS has become one of the most deeply studied material combination also in the forms of quantum dots [19,36], and tetrapods [75] besides NRs [105].

Recently, a low threshold ASE from CdSe/CdS/ZnS quantum dots [79-82] and CdSe/CdS NRs [86] pumped via TPA mechanism was demonstrated. The tunability of electron and hole wavefunctions overlap in this material system has

been discussed in the literature for both entangled photon generation [106] and nanocrystal lasing applications [92]. However, ASE from the same material system of CdSe/CdS NRs with Type-I-like, Type-II-like and quasi Type-II-like behaviors under TPA-based pumping has not been demonstrated. In this chapter, as a result of exciton-exciton interaction engineering with core/shell size adjustments, we report on the Type-tunability feature resulting in blue-shifting, red-shifting and non-shifting ASE with respect to spontaneous emission of NRs pumped with TPA mechanism. We will then provide the verification of the Type attributions of different size NRs by checking their time-resolved decay dynamics where the NRs with Type-II-like behavior has significantly longer decay lifetimes as a consequence of decreased electron/hole wavefunction overlap, and hence, oscillator strength compared to Type-I-like NRs.

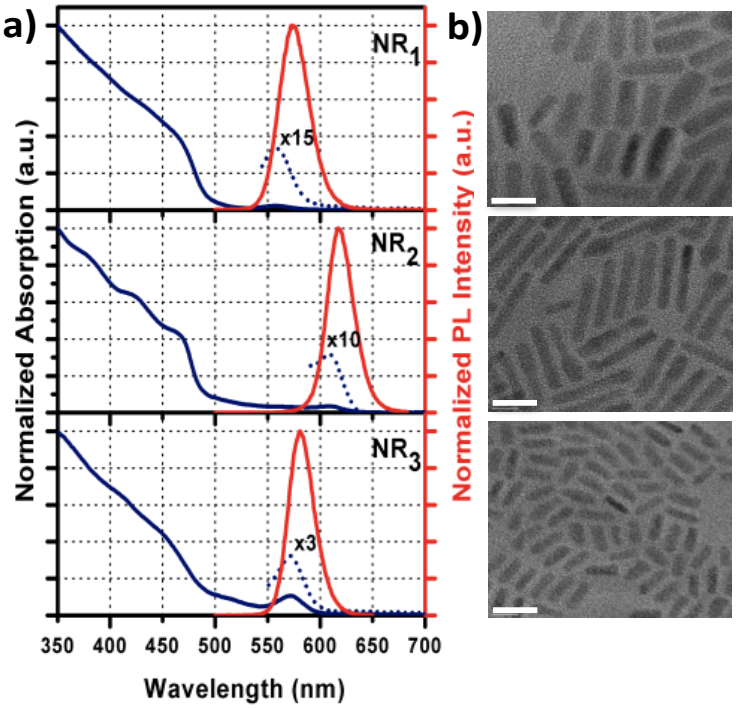

Figure 4.2.1. a) Absorption and photoluminescence spectra of CdSe/CdS core/shell NRs having different core sizes and rod lengths along with b) high resolution transmission electron microscopy (TEM) images (scale bars = 10 nm).

In this study, we synthesized highly efficient and stable core seeded CdSe/CdS core/shell NRs having different core sizes and rod lengths using a well-known recipe from the literature [107]. As can be seen from the TEM images in Figure 4.2.1(b), they exhibit highly crystalline structure with narrow size distribution, which results in high quantum efficiency (>40%) for NRs. Owing to very small lattice mismatch between CdSe and CdS (3.9%) and the fact that CdSe/CdS NRs were grown epitaxially, it is not easy to differentiate CdSe and CdS regions and confirm growth of CdS rod region by using the TEM images. However, the formation of CdS rod surrounding CdSe core can be confirmed easily from the sharp increase in the absorption spectrum around 400-500 nm region (Figure 4.2.1(a)), which corresponds to the band gap of wurtzite CdS. In addition, with increasing rod length, this signature of rod absorption becomes more dominant and makes significant contribution to the absorption cross-section. Thanks to this very high absorption of mainly rod-shaped shell region of NRs, it was also shown that they are very good two-photon sensitizers, which is highly desirable for optical gain materials [98].

4.2.1 Amplified Spontaneous Emission Experiments of NRs

For the optical gain study of NR samples, similar to the optical gain study of QD samples discussed in the previous chapter, all three high quality close-packed films were prepared by drop-casting of highly concentrated solutions (100mg/mL) of CdSe/CdS NRs on bare quartz substrates. The experimental conditions are also similar to that of the QD-ASE work. The films were pumped with 200 fs laser pulses at a 1 kHz repetition rate and the central wavelength of 800 nm and the laser beam was focused to a spot size of 15.7 mm^2 on samples by using a cylindrical lens.

The excitation intensity dependent emission spectrum of CdSe/CdS NR_1 sample having a core diameter of 3.8-4.0 nm and a rod length of 30 nm is given in Figure 4.2.1.1 [108]. At low excitation intensities, only spontaneous emission was observed having a peak at 632 nm with a full-width-at-half-maximum (FWHM) value of 34 nm. However, when the excitation intensity exceeds the threshold value (7.5 mJ/cm^2), a slightly red-shifted ASE peak emerged at 634 nm with a FWHM value of 7 nm, which is very low as would be expected from an ASE process. When compared to the most commonly used QDs such as CdSe/ZnS and CdSe/CdS/ZnS, the optical gain threshold value can be said to be very low, which can be attributed to the increased absorption cross-section.

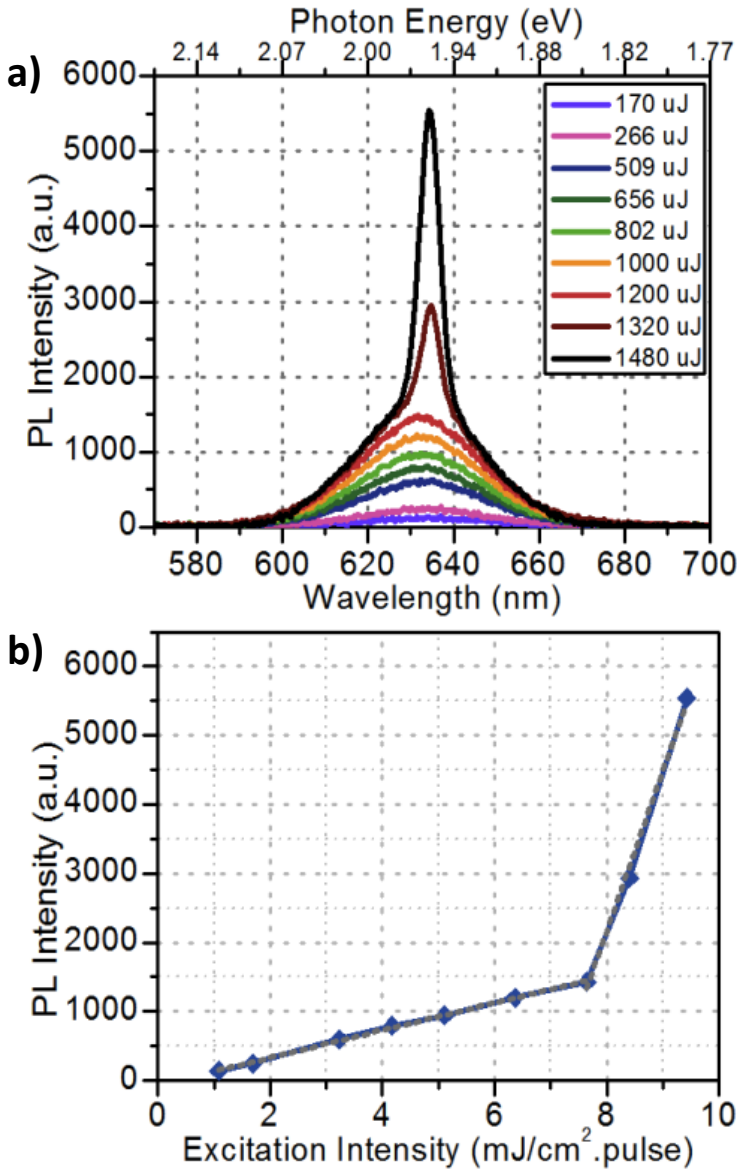

Figure 4.2.1.1. a) Photoluminescence emission spectra of highly concentrated close-packed film of CdSe/CdS NR_1 sample under different excitation pulse intensities and b) excitation pulse intensity dependence of the emission at the ASE peak position of CdSe/CdS NR_1.

4.2.2 Demonstration of Type-Tunability Feature of CdSe/CdS Nanorods in Their Amplified Spontaneous Emission Spectra

It was shown that, owing to a lower energy barrier for electrons in CdSe/CdS core/shell material systems, Type-tunable electronic structure from Type-I to Type-II was achieved by changing the core size and rod length [60,92]. Therefore, in order to figure out the effect of different electronic structures on optical gain performance from the same material system, we designed and synthesized CdSe/CdS NRs with different core sizes and shell thicknesses. Also, we demonstrated for the first time Type-tunability of the ASE peak originating from biexciton emission with respect to spontaneous emission via engineering attractive vs. repulsive nature of exciton-exciton interactions in the NRs. For example, as a result of the smaller core size of NR_1, electrons were not confined to the CdSe core and partial separation of electron and hole wavefunctions took place. Therefore, when we optically pumped the highly concentrated close-packed film of NR_1, we observed Type-II-like behavior with an approximately 9 nm blue-shifted ASE peak due to repulsive exciton-exciton interaction (Figure 4.2.2.1) [21,95]. On the other hand, when the core size was increased like in the case of NR_2, the leakage of electrons to the CdS shell decreased. Therefore, Type-I-like behavior was achieved with a 4 nm red-shifted ASE peak from the high quality film of NR_2 owing to attractive exciton-exciton interaction. Finally, we showed that attractive vs. repulsive nature of exciton-exciton interaction can be modified not only by changing the core size but also the rod length. As can be seen from Figure 4.2.2.1(c), a non-shifted ASE peak was achieved from the NR_3 having a larger core size and a longer rod length, owing to the balanced attractive and repulsive exciton-exciton interaction. For this sample, looking at only the core size would suggest that the NRs should exhibit Type-I like behavior and looking at the shell length would tell us that the NRs should

behave like Type-II. The balance between dominances of these two localization regimes resulted in neither attractive nor repulsive X-X interaction.

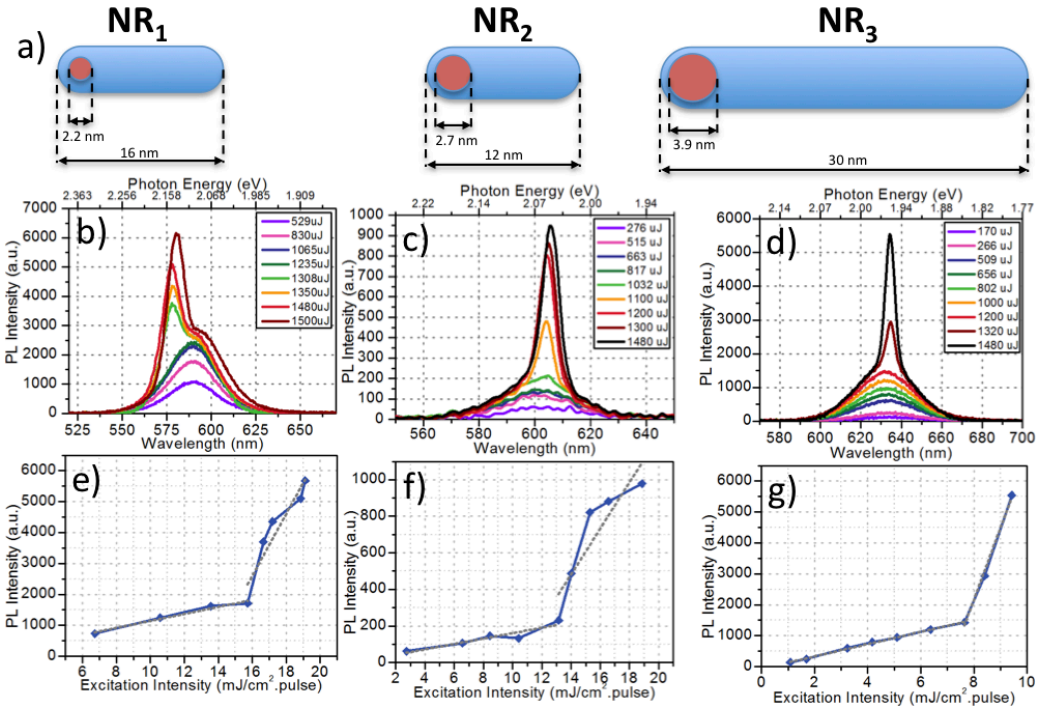

Figure 4.2.2.1. a) Schematic illustration of CdSe/CdS core/shell NRs proportional to their real size. b) - d) Excitation intensity dependent emission spectra of NR_1 (with blue-shifted ASE peak), NR_2 (with red-shifted ASE peak), and NR_3 (with ASE peak at the same position as the spontaneous emission), respectively. e) - g) Excitation pulse intensity dependences of emissions at the ASE peak positions of NR_1, NR_2, and NR_3, respectively.

As can be seen in Figure 4.2.2.1, the lowest ASE threshold is observed for NR_3 sample where the ASE peak and spontaneous emission peak are at the same wavelength. This can be because the ASE can be both from BX and X states in these NRs as a very good example of the direct effect of X-X interaction engineering on ASE threshold. The other contributing factor for low ASE threshold observation from NR_3 sample can be the high TPA cross-section of these NRs compared to the other in association with their large sizes.

4.2.3 Verification of Type Attributions of Nanorods by Independent Time-Resolved Fluorescence Experiments

In order to verify the hypothesis on electron wavefunction localization engineering stated above and gain more insight into the electronic band structure of core seeded CdSe/CdS NRs with different core sizes and rod lengths, we conducted TRF by using insolution samples of NRs with lower concentrations under lower excitation intensities to make sure the NRs are occupied with at most single excitons. In literature, for the bare CdSe core nanocrystals, decrease in radiative lifetime was demonstrated with decreasing core size [109]. In addition, for the CdSe/CdS core/shell NRs, increased lifetime was reported with increasing rod length. In contrast to the literature, we observed the longest radiative lifetime (~30 ns) from the NR_1 sample with the smaller core size and shorter rod length, which can be attributed to the Type-II behavior. In other words, owing to the smaller core size in NR_1, electrons were delocalized over the CdS shell region and with the decreased wavefunction overlap of the electron and the hole, a longer radiative lifetime was observed (Figure 4.2.3.1). On the other hand, with the increased core size, leakage of electrons to the shell region was reduced and a shorter radiative lifetime was measured as a result of increased electron and hole wavefunction overlap, which can be explained by the Type-I behavior.

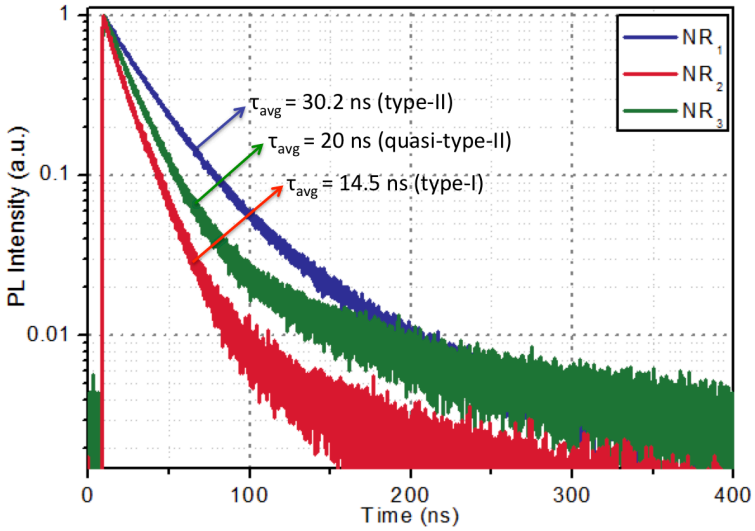

Figure 4.2.3.1. TRF decay curves of the NRs together with average least chi-square fitting lifetimes.

Chapter 5

Multi Exciton Generation and Recombination in CdHgTe Quantum Dots

As stated in the previous chapters, MEG concept, generating two excitons upon absorption of a single photon, has a potential to revolutionize the fields of photovoltaics and photodetection. In this chapter, we report a practical utilization of this concept in photosensors, which is one of the first successful demonstrations of real-life application of MEG. First, we demonstrate the presence of MEG event in CdHgTe QDs in solution form. Then we provide the experimental sensitivity measurements and the enhancement due to MEG event in CdHgTe QD-based photosensors.

5.1 Observation of Multi Exciton Generation and Recombination in CdHgTe Quantum Dots

Because of the conservation of energy principle, in order to be able to generate multiple excitons from a single photon absorption event, the incoming photon must have at least twice the energy bandgap of the absorber material. Therefore, considering the limited photon energy of the sunlight spectrum, the QDs that would be used in photosensing employing MEG concept should have a bandgap

in the near-infrared or infrared region. To date, the most commonly employed QDs in MEG studies are PbSe and PbS QDs [5,110,111]. However, $Cd_xHg_{1-x}Te$ QDs can also be very strong candidates for such studies because the composition adjustability brings another degree of freedom on the design of the electronic structure of QDs. Furthermore, Pb-based QDs have some long-term stability issues that CdHgTe QDs do not. Therefore, we based our MEG device study on CdHgTe QDs and demonstrated the presence of MEG on CdHgTe QDs before the device implementation.

In CdHgTe QDs, the generated BXs decay nonradiatively via Auger recombination (AR), which has a lifetime two to three orders of magnitude shorter than that of the radiative recombination of these QDs. Therefore, the presence of this very fast AR decay term in the global decay of QDs can be considered to be the signature of MEG event, as is the case for many works in the literature. It is very critical here to keep in mind that BXs are not the only ones that recombine via AR and trions can also recombine via AR, causing a false MEG signature in the overall decay of TRF measurements. This has been the main source for the confusions existed among the MEG researchers. In this study, we kept this in mind and observed that stirring the in-solution sample, avoiding the generation of trions, did not change our TRF decays. Therefore, we can say that in our experiments, the photocharging effect was not a problem.

In this study, we used in solution sample of aqueous CdHgTe QDs with a bandgap of ca. 1.48 eV (835 nm), whose PL emission spectrum and the transmission electron microscopy image are presented in Figure 5.1.1. The QDs were synthesized via the method previously published [112]. The concentration of the sample was kept at minimum within the experimentally feasible region in order to avoid nonradiative energy transfer among the QDs in the ensemble. The TRF experiments were conducted using Horiba Jobin Yvon TCSPC setup (FL-

1057) with variable-wavelength pulsed excitation LED sources. In order to avoid generation of BXs by multiple photon absorption events and be sure that the generated BXs are from single photon absorption events, we kept the excitation intensity as low as possible during the experiments.

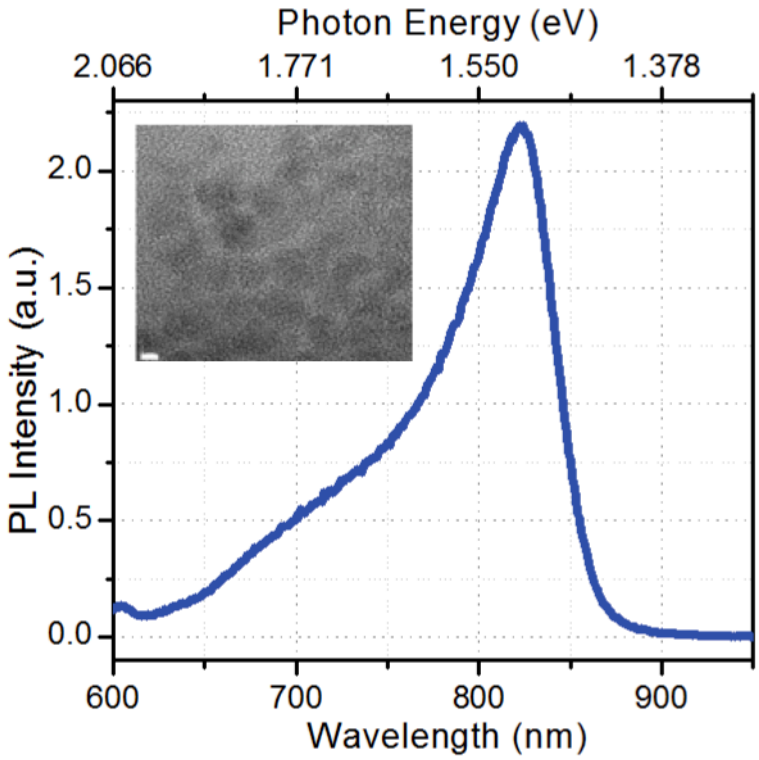

Figure 5.1.1. PL emission spectrum and transmission electron microscopy image of CdHgTe QDs used in this study. The size bar corresponds to 2 nm.

The excitation photon energy threshold for MEG is $\hbar\omega_{th} = \left(2 + m_e/m_h\right) \cdot E_g$ as reported in the literature [9,52,113]. The dependence of the threshold on electron and hole effective masses comes from the fact that excess energy of the incoming photon is shared between the electron and hole inversely proportional to their effective masses. Since MEG occurs only when one of the charge carriers have kinetic energy as much as the bandgap, the MEG threshold is above twice the bandgap. CdHgTe can be said to be advantageous also in terms

of the MEG threshold because the hole effective mass is much bigger than the electron effective mass resulting in an MEG threshold $\hbar\omega_{th} \approx 2 \cdot E_g$. Since the bandgap of CdHgTe QDs used here is 1.48 eV, the expected MEG threshold is about 2.96 eV.

The results of the TRF experiments under various excitation photon energies are provided in Figure 5.1.2 [114]. Although the emergence of very short lifetime AR for photon energies above bandgap is not vey visible in Figure 5.1.2(a), a closer look at the first 30 ns part of the decays in Figure 5.1.2(b) clearly reveals the existence of fast decay term for the photon energy 3.18 eV. As expected from 2.96 eV MEG threshold value, for the case with excitation photon energy 2.82 eV, the fast decay term is not observed. This consistency between MEG threshold expectation and the experimental photon energy threshold for the fast decay peak suggests claim that this fast peak is due to MEG event.

An important point that should be noted here is that the pulse widths of the excitation sources are 1.3-1.4 ns while the fast decay lifetime that we attribute to AR is expected to be on the order of 100s of picoseconds. Therefore, the wide pulse of the excitation LED smears the original fast decay out. In order to extract the lifetime of the fast decay and make quantitative comments, the fitting of the decays was made with reconvolution mode.

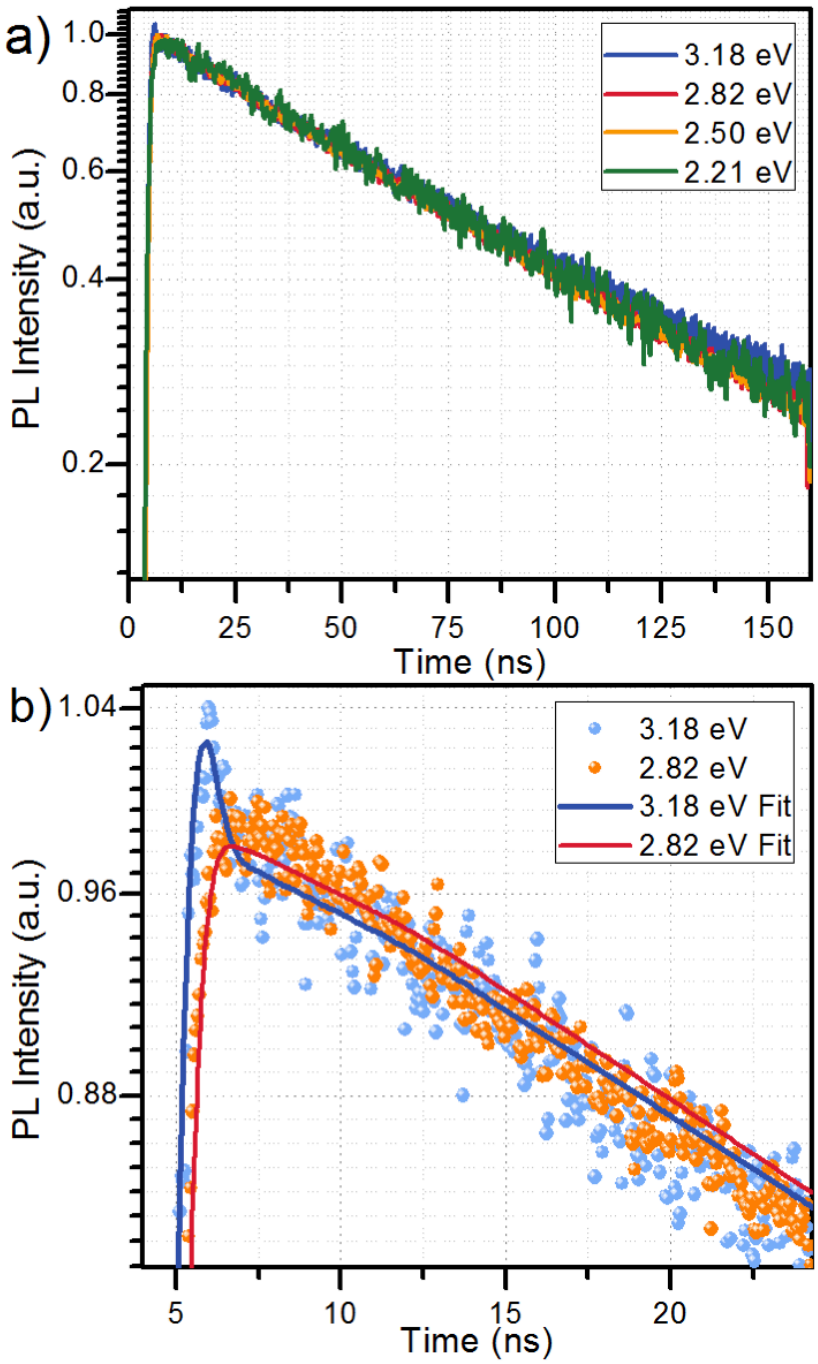

Figure 5.1.2. TRF decay results of aqueous CdHgTe QDs at 820 nm (1.512 eV) excited at various excitation photon energies. a) The entire TRF decay of the sample excited at four different photon energies, b) the first 30 ns of the decay of the sample including the least chi-squared fits for two excitation photon energies, one causing MEG and one not causing MEG.

Table 5.1.1. Fitting coefficients and lifetimes of photoluminescence decay curves shown in Figure 5.1.2.

	A_1	τ_1 (ns)	A_2	τ_2 (ns)
2.21 eV	1.60×10^{-3} ($\pm4.7\times10^{-6}$)	104.0 ($\pm714.2\times10^{-3}$)	--	--
2.50 eV	5.75×10^{-5} ($\pm4.0\times10^{-6}$)	104.6 ($\pm188.9\times10^{-3}$)	--	--
2.82 eV	1.57×10^{-2} ($\pm6.8\times10^{-4}$)	107.0 ($\pm125.3\times10^{-3}$)	8.63×10^{-3} ($\pm6.6\times10^{-4}$)	0.1157 ($\pm7.4\times10^{-3}$)
3.18 eV	1.11×10^{-2} ($\pm7.3\times10^{-6}$)	104.4 ($\pm194.2\times10^{-3}$)	5.31×10^{-2} ($\pm8.9\times10^{-4}$)	0.1160 ($\pm11.7\times10^{-3}$)

The fitting results of these photoluminescence curves are given in Table 5.1.1. As can be seen in the table, these decay curves are fitted using one-exponential decay formula for the cases without MEG and two-exponential decay formula for the cases with MEG. For all the excitation photon energy cases, the lifetime values are stable around 104 ns for the slow decay component and 116 ps for the fast decay component. Here, the long-lifetime decay term belongs to single exciton recombination of QDs and the short lifetime can be attributed to AR. The lifetime of AR turned out to be sub-nanosecond as expected.

It should also be noted here that the amplitude weight of the fast decay component with respect to the coefficient of slow decay component is higher for the photon energy of 3.18 eV than that of 2.82 eV. This means that the increasing photon energy increases the probability of MEG as would be intuitively expected.

5.2 Practical Utilization of Multi Exciton Generation in Photosensing Device Applications

To benefit from the generated multi excitons in photosensing applications, we fabricated photosensors, called light-sensitive nanocrystal skins (LS-NSs) [115,116], employing CdHgTe QDs as the absorber material. For these experiments, we to fabricated LS-NSs with two CdHgTe QDs with different sizes and bandgaps.

5.2.1 Photosensor Device Fabrication and Operation Principles

The LS-NS device structure is presented in Figure 5.2.1.1. The device fabrication starts with the cleaning of indium tin oxide (ITO)-coated glass substrate with 1 × 0.75 cm area. After cleaning the ITO substrate, 50 nm thick highly dielectric HfO_2 is deposited via atomic layer deposition (ALD). The pulsed water application in ALD process preferentially coats hydrophilic surfaces, which helps to improve the dip-coated film quality. Subsequently, in order to deposit highly close-packed monolayer of QDs on the substrate, poly (diallyldimethylammonium chloride) (PDDA) and poly (sodium 4-styrenesulfonate) (PSS) bilayers were dip-coated to build four bilayers using layer-by-layer assembly [117]. Then, the device was dipped into the low concentration solution of CdHgTe QDs and a monolayer of QDs that will serve as the absorber layer was later coated. Finally, Al contact was laid down immediately on top of the CdHgTe QDs monolayer by using electron beam evaporator.

In this way, we fabricated devices with two different size QDs. One of these QDs, whose MEG behavior is discussed in the previous section, has a bandgap

of 1.48 eV (835 nm) and its ligand is mercaptoacetic acid (MPA). The other one has a badgap of 1.31 eV (950 nm) and its ligand is thioglycolic acid (TGA).

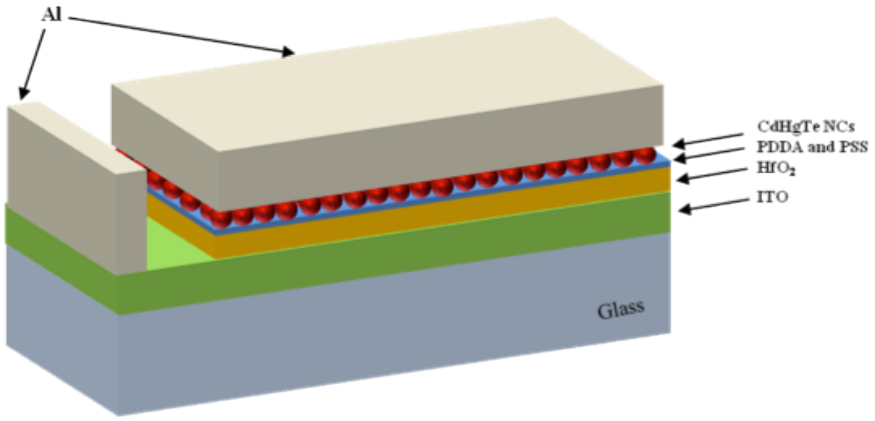

Figure 5.2.1.1. LS-NS device structure.

The operation of this device is based on the photovoltage buildup across the device upon photon absorption. After the photons are absorbed by the QD layer, the generated excitons are dissociated. Then, Al serves as the hole acceptor layer and the holes are transported through the Al contact while the electrons get trapped within the QD layer. Therefore, the whole device acts like a capacitor whose stored charge is determined by the number of absorbed photons. The stored charge amount can be read as the voltage buildup on the device as the output of the photodetector. Note that there is no need for external bias application to operate the device.

5.2.2 Demonstration of Multi Exciton Generation on Photosensor Device

For the demonstration of MEG in our LS-NS devices, similar to the previous part for determining the existence of MEG in CdHgTe dispersion sample, we basically varied the excitation photon energy and measured the voltage buildup across the device. In these measurements, we used a Xenon lamp source that

produces continuous excitation over a wide spectral range (350 – 550 nm). The excitation wavelengths of the experiments were chosen with a monochromator. Both static and dynamic voltage buildup of the device were measured with a semiconductor parameter analyzer (Agilent, B1500A). Considering the absorbance of CdHgTe QDs, we adjusted the excitation intensity with an attenuator in order to make sure that at every excitation wavelength the numbers of absorbed photons by the devices are the same.

In the experiments, after we turn on the excitation on the sample, we waited until the voltage buildup reached its max value. Then we turned the illumination off and let the device get discharged through a 200 MΩ resistance. The corresponding time-dependences of the devices are shown in Figure 5.2.2.1(a). After obtaining the peak voltage buildup values, we calculated the sensitivity values using the formula: $S = \frac{V_{buildup}}{P_{inc}}$ where $V_{buildup}$ is the peak voltage value that the device reached (Figure 5.2.2.1(a)) and P_{inc} is the incident photon number. These sensitivities of the LS-NS devices with respect to incident photon energy are depicted in Figure 5.2.2.1(b). As can be seen in the figure for the device with MPA ligand QDs (with a bandgap corresponding to 835 nm), there is a clear threshold at ca. 425 nm above which the sensitivity jumps. This threshold value of 425 nm is very close to what we found in the previous part as MEG threshold. On the other hand, for the device with TGA coated QDs (with a bandgap of 950 nm) the MEG threshold for sensitivity of the device is 475 nm, as shown in Figure 5.2.2.1(b). Thus, this threshold on TGA-based QDs is also consistent with the expected MEG threshold of about twice the bandgap of the QDs. These consistencies can be considered as the evidences of the abrupt sensitivity changing in the spectral response of LS-NS devices as a consequence of MEG events in the QDs.

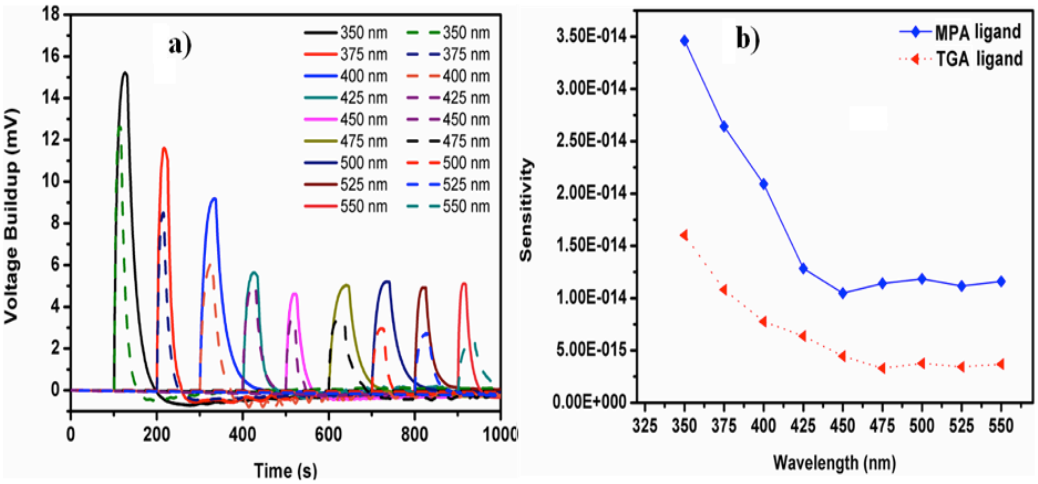

Figure 5.2.2.1. a) Voltage buildup and discharging dynamics of devices with MPA- ligand QDs (dashed lines) and TGA-ligand QDs (solid lines) and b) spectral sensitivity performance of two devices.

It should also be noted here that, in addition to MEG event, increasing the photon energy is expected to gradually increase the sensitivities of LS-NS devices because these devices operate based on the electron trapping within the QD absorber layer. Since hot electrons will be easier to get trapped in the trap sites of the QD layer, the devices are more sensitive to higher photon energy excitation. It is this contribution in sensitivity that causes 3-fold higher sensitivity for the device with MPA-based QDs, although MEG alone can cause at most 2-fold sensitivity improvement. Therefore, this contribution should be kept in mind. However, the abrupt sensitivity enhancements at the spectral positions in perfect agreement with MEG expectancies cannot be explained with this trapping mechanism. Independent TRF measurements provided in the previous chapter also verify our attribution for the part of the device performance enhancement to MEG.

Chapter 6

Conclusion

In this thesis, we reviewed our recent findings and observations on the concepts of multi exciton generation (MEG) and multi exciton recombination (MER) in colloidal semiconductor nanocrystal quantum dots with various material, size and shape combinations. Besides the fundamental understanding point of view, we aimed also at proof-of-concept demonstrations of application possibilities of these concepts by using the know-how we developed during the fundamental studies.

First, we successfully resolved and identified the radiative biexciton (BX) recombination events in the presence of photocharging in the solid ensembles of CdSe/CdS QDs with near-unity quantum yield. We distinguished the radiative exciton (X), BX, and trion recombination events by systematically analyzing the multi-exponential decay components of the overall TRF decay throughout the entire emission spectrum. Our experiments on three different QD samples with different core sizes revealed the dependence of spectral BX recombination behavior on the carrier localizations in the QDs, which can be conveniently tuned to engineer the X-X interaction energy. We introduced the integrated TRF terms $A_i\tau_i$ to reveal the spectrally resolved kinetics of multi-exciton recombination, which is otherwise spectrally unresolved in the ensemble of QD solids. The spectral overlap of different events in MER normally makes the ensemble study of these events impossible and single QD measurements would

be needed in order to resolve and see the distinct spectral behaviors of different events. However, the analysis method devised here has enabled us to eliminate "the ensembling effect" because we relied on the characteristic decay lifetimes of the events to distinguish them from one another. Therefore, we could see the individual spectral behaviors of the events although they are spectrally mixed. For this part of the thesis, we provided either independent experimental evidence we obtained ourselves or supporting results from the literature for each and every comment we made during the resolution of excitonic events taking place in the ensemble QD solids. We believe that these findings and discussions fill an important gap in understanding the spectral dynamics of MER in these QD solids and their behavior under the photocharging effects. In addition to the results and conclusions about excitonic species in the QDs investigated in this work, we reckon that the systematic analysis approach devised in this study can be an important enabling tool that can help us study not only the radiative recombination events in any kind of ensemble samples consisting of one Type of emitters but also their nonradiative recombination events.

In the second part of thesis, we demonstrated high performance Type-tunable amplified spontaneous emission (ASE) from near-unity quantum yield CdSe/CdS core/shell QDs excited via two-photon excitation mechanism. The two-photon absorption (TPA) cross-section of CdSe/CdS QDs is found to strongly support the assertion that these QDs are promising for TPA applications. The absolute and relative spectral tunabilities of ASE for Type-I-like, Type-II-like, and quasi-Type-II operations (with adjustable ASE shift from spontaneous emission) from the same material system were, for the first time, shown as other exceptional features of CdSe/CdS QDs, which make them very strong competitors against other emitters for QD lasing applications. Type-tunability of CdSe/CdS QDs through X-X interaction engineering can be considered to be a promising method for optimizing the lasing performances of

future QD lasers. With proper X-X interaction engineering, it is possible to obtain ASE at a certain wavelength on the lower or higher energy tail of the spontaneous emission of QDs. For future applications, high performance ASE through TPA process from these QDs, together with their Type-tunability feature, is a good indicator for the feasibility of QD lasing via two-photon pumping.

In the next part of the thesis, we showed that, with their giant TPA coefficients, CdSe/CdS nanorods (NRs) are the strongest candidates for lasing applications with two-photon optical pumping. Moreover, owing to their Type tunable electronic configuration (Type-I vs. Type-II), blue-shifted, non-shifted and red-shifted ASE peak with respect to spontaneous emission was achieved via tuning exciton-exciton interaction from the CdSe/CdS core/shell material system, which could prove useful when maximizing their optical gain performance through, for example, reducing re-absorption processes. Furthermore, we verified the Type-tunability of CdSe/CdS NRs with in-solution TRF measurements. These results indicate that, with high TPA coefficient and ability to control the ASE peak shift, CdSe/CdS NRs are very promising candidates for practical lasing applications.

In the last part of the thesis, for the first time in the literature, we showed the generation of BXs with the absorption of a single photon in aqueous CdHgTe QDs with bandgaps in the near-infrared region. Besides the demonstration of MEG in freestanding QDs, we designed and fabricated photosensors dubbed light sensitive nanocrystal skins using these CdHgTe QDs on which we obtained significant performance enhancements in the sensitivity. As one of the very first demonstrations of MEG concept in real-life application of photosensing, this study can be considered as a proof-of-concept demonstration of how strong and effective MEG concept can be if engineered properly.

In conclusion, our goal has been to comprehensively study MEG/MER in colloidal QDs and contribute to the related fields not only by resolving uncomprehended aspects of these concepts, but also by proposing possible new application areas with novel engineering approaches.

6.1 Scientific Contributions

- Cihan A. F., Hernandez-Martinez L. P., Kelestemur Y., and Demir H. V., "Observation of Biexcitons in Nanocrystal Solids in the Presence of Photocharging", **ACS Nano**, 7, 4799, 2013.
- Cihan A. F., Kelestemur Y., Guzelturk B., Yerli O., Kurum U., Yaglioglu H. G., Elmali A., and Demir H. V., "Attractive *versus* Repulsive Excitonic Interactions of Colloidal Quantum Dots Control Blue- to Red-Shifting (and Non-Shifting) Amplified Spontaneous Emission", submitted, 2013.
- Kelestemur Y., Cihan A. F., Guzelturk B., and Demir H. V., "Type Tunable Amplified Spontaneous Emission from Core Seeded CdSe/CdS Core/Shell Nanorods via Exciton-Exciton Engineering", in submission, 2013.
- Akhavan S., Cihan A. F., Bozok B., and Demir H. V., "Exciton Funneling Nanocrystal Skins for Photosensing", submitted, 2013.
- Cihan A. F. et al., "Multi Exciton Generation and Utilization in Photosensors Employing Quantum Dots", in preparation, 2013.
- Cihan A. F., Kelestemur Y., Guzelturk B., and Demir H. V., "Type-tuning of quasi-Type-II CdSe/CdS seeded core/shell nanorods: Type-I vs. Type-II", ***CLEO 2013,*** San Jose, CA, USA, 9-14 Jun. 2013.

- Kelestemur Y., Cihan A. F., Guzelturk B., Yerli O., Kurum U., Yaglioglu H. G., Elmali A., and Demir H. V., "Blue- and red-shifted amplified spontaneous emission from quasi-Type II CdSe/CdS core/shell quantum dots with two-photon optical pumping", ***CLEO 2013,*** San Jose, CA, USA, 9-14 Jun. 2013.

- Cihan A. F., Hernandez-Martinez L. P., Kelestemur Y., and Demir H. V., "Observation of Biexcitons in the Presence of Trions Generated via Sequential Absorption of Multiple Photons in Colloidal Quantum Dot Solids", ***IEEE Photonics Conference 2012***, Burlingame, San Francisco, CA, USA, 23-27 Sep. 2012.

Bibliography

[1] A. F. Cihan, P. L. Hernandez Martinez, Y. Kelestemur, E. Mutlugun, and H. V. Demir, "Observation of biexcitons in nanocrystal solids in the presence of photocharging" *ACS Nano*, vol. 7, pp. 4799–4809, 2013.

[2] W. Shockley and H. J. Queisser, "Detailed Balance Limit of Efficiency of p-n Junction Solar Cells" *J. Appl. Phys.*, vol. 32, no. 3, pp. 510, 1961.

[3] V. I. Klimov, "Detailed-balance power conversion limits of nanocrystal-quantum-dot solar cells in the presence of carrier multiplication" *Appl. Phys. Lett.*, vol. 89, p. 123118, 2006.

[4] V. I. Klimov, "Spectral and dynamical properties of multiexcitons in semiconductor nanocrystals" *Ann. Rev. of Phys. Chem.*, vol. 58, pp. 635–73, 2007.

[5] R. D. Schaller and V. I. Klimov, "High Efficiency Carrier Multiplication in PbSe Nanocrystals: Implications for Solar Energy Conversion" *Phys. Rev. Lett.*, vol. 92, pp. 186601, 2004.

[6] J. A. McGuire, J. Joo, J. M. Pietryga, R. D. Schaller, and V. I. Klimov, "New aspects of carrier multiplication in semiconductor nanocrystals" *Acc. Chem. Res.*, vol. 41, pp. 1810–1819, 2008.

[7] L. A. Padilha, J. T. Stewart, R. L. Sandberg, W. K. Bae, W.-K. Koh, J. M. Pietryga, and V. I. Klimov, "Aspect ratio dependence of Auger recombination and carrier multiplication in PbSe nanorods" *Nano Lett.*, vol. 13, pp. 1092–1099, 2013.

[8] V. I. Klimov, "Mechanisms for Photogeneration and Recombination of Multiexcitons in Semiconductor Nanocrystals : Implications for Lasing and Solar Energy Conversion" *J. Phys. Chem. B*, vol. 110, pp. 16827–16845, 2006.

[9] A. J. Nozik, "Multiple exciton generation in semiconductor quantum dots" *Chem. Phys. Lett.*, vol. 457, pp. 3–11, 2008.

[10] A. Shabaev, A. L. Efros, and A. J. Nozik, "Multiexciton generation by a single photon in nanocrystals" *Nano Lett.*, vol. 6, pp. 2856–63, 2006.

[11] A. J. Nozik, “Separating multiple excitons” *Nat. Photon.*, vol. 6, pp. 272–273, 2012.

[12] D. J. Binks, “Multiple exciton generation in nanocrystal quantum dots--controversy, current status and future prospects” *Phys. Chem. Chem. Phys.*, vol. 13, pp. 12693–12704, 2011.

[13] J. B. Sambur, T. Novet, and B. A. Parkinson, “Multiple Exciton Collection in a Sensitized Photovoltaic System” *Science*, vol. 330, pp. 63–66, 2010.

[14] O. E. Semonin, J. M. Luther, S. Choi, H.-Y. Chen, J. Gao, A. J. Nozik, and M. C. Beard, “Peak external photocurrent quantum efficiency exceeding 100% via MEG in a quantum dot solar cell” *Science*, vol. 334, pp. 1530–1533, 2011.

[15] W. Witzel, A. Shabaev, C. Hellberg, V. Jacobs, and A. Efros, “Quantum Simulation of Multiple-Exciton Generation in a Nanocrystal by a Single Photon” *Phys. Rev. Lett.*, vol. 105, pp. 137401, 2010.

[16] R. J. Ellingson, M. C. Beard, J. C. Johnson, P. Yu, O. I. Micic, A. J. Nozik, A. Shabaev, and A. L. Efros, “Highly efficient multiple exciton generation in colloidal PbSe and PbS quantum dots” *Nano Lett.*, vol. 5, pp. 865–71, 2005.

[17] R. D. Schaller, J. M. Pietryga, S. V. Goupalov, M. a. Petruska, S. a. Ivanov, and V. I. Klimov, “Breaking the Phonon Bottleneck in Semiconductor Nanocrystals via Multiphonon Emission Induced by Intrinsic Nonadiabatic Interactions,” *Phys. Rev. Lett.*, vol. 95, pp. 1–4, 2005.

[18] O. V. Prezhdo, “Multiple excitons and the electron–phonon bottleneck in semiconductor quantum dots: An ab initio perspective” *Chem. Phys. Lett.*, vol. 460, pp. 1–9, 2008.

[19] F. García-Santamaría, Y. Chen, J. Vela, R. D. Schaller, J. A. Hollingsworth, and V. I. Klimov, “Suppressed Auger Recombination in ‘ Giant ’ Nanocrystals Boosts Optical Gain Performance” *Nano Lett.*, vol. 9, pp. 3482–3488, 2009.

[20] V. I. Klimov, A. A. Mikhailovsky, S. Xu, A. Malko, J. A. Hollingsworth, C. A.Leatherdale, H.-J. Eisler, and B. M. G, “Optical Gain and Stimulated

Emission in Nanocrystal Quantum Dots" *Science*, vol. 290, pp. 314–317, 2000.

[21] V. I. Klimov, S. a Ivanov, J. Nanda, M. Achermann, I. Bezel, J. A. McGuire, and A. Piryatinski, "Single-exciton optical gain in semiconductor nanocrystals" *Nature*, vol. 447, pp. 441–446, 2007.

[22] C. Dang, J. Lee, C. Breen, J. S. Steckel, S. Coe-Sullivan, and A. Nurmikko, "Red, green and blue lasing enabled by single-exciton gain in colloidal quantum dot films" *Nat. Nano.*, vol. 7, pp. 335–339, 2012.

[23] B. M. Kazes, D. Y. Lewis, Y. Ebenstein, T. Mokari, and U. Banin, "Lasing from Semiconductor Quantum Rods in a Cylindrical Microcavity" *Adv. Mater.*, vol. 14, pp. 317–321, 2002.

[24] J. T. Stewart, L. A. Padilha, M. M. Qazilbash, J. M. Pietryga, A. G. Midgett, J. M. Luther, M. C. Beard, A. J. Nozik, and V. I. Klimov, "Comparison of Carrier Multiplication Yields in PbS and PbSe Nanocrystals: The Role of Competing Energy-Loss Processes" *Nano Lett.*, vol. 12, pp. 622–628, 2012.

[25] C. M. Isborn and O. V. Prezhdo, "Charging Quenches Multiple Exciton Generation in Semiconductor Nanocrystals: First-Principles Calculations on Small PbSe Clusters" *J. Phys. Chem. C*, vol. 113, pp. 12617–12621, 2009.

[26] S. J. Kim, W. J. Kim, Y. Sahoo, A. N. Cartwright, and P. N. Prasad, "Multiple exciton generation and electrical extraction from a PbSe quantum dot photoconductor" *Appl. Phys. Lett.*, vol. 92, pp. 031107, 2008.

[27] R. D. Schaller, M. A. Petruska, and V. I. Klimov, "Tunable Near-Infrared Optical Gain and Amplified Spontaneous Emission Using PbSe Nanocrystals" *J. Phys. Chem. B*, vol. 107, pp. 13765–13768, 2003.

[28] G. Nootz, L. Padilha, L. Levina, V. Sukhovatkin, S. Webster, L. Brzozowski, E. Sargent, D. Hagan, and E. Van Stryland, "Size dependence of carrier dynamics and carrier multiplication in PbS quantum dots" *Phys. Rev. B*, vol. 83, p. 155302, 2011.

[29] A. M. Smith and S. Nie, "Bright and compact alloyed quantum dots with broadly tunable near-infrared absorption and fluorescence spectra through mercury cation exchange" *J. Am. Chem. Soc.*, vol. 133, pp. 24–26, 2011.

[30] W. K. Bae, K. Char, H. Hur, and S. Lee, “Single-Step Synthesis of Quantum Dots with Chemical Composition Gradients” *Chem. Mater.*, vol. 20, pp. 531–539, 2008.

[31] R. Xie, U. Kolb, J. Li, T. Basche, and A. Mews, “Synthesis and Characterization of Highly Luminescent CdSe-Core CdS/Zn0.5Cd0.5S/ZnS Multishell Nanocrystals” vol. 127, *J. Am. Chem. Soc.*, pp. 7480–7488, 2005.

[32] A. B. Greytak, P. M. Allen, W. Liu, J. Zhao, E. R. Young, Z. Popović, B. J. Walker, D. G. Nocera, and M. G. Bawendi, “Alternating layer addition approach to CdSe/CdS core/shell quantum dots with near-unity quantum yield and high on-time fractions” *Chem. Sci.*, vol. 3, pp. 2028–2034, 2012.

[33] J. J. Li, Y. A. Wang, W. Guo, J. C. Keay, T. D. Mishima, M. B. Johnson, and X. Peng, “Large-scale synthesis of nearly monodisperse CdSe/CdS core/shell nanocrystals using air-stable reagents via successive ion layer adsorption and reaction” *J. Am. Chem. Soc.*, vol. 125, pp. 12567–12575, 2003.

[34] B. Mahler, P. Spinicelli, S. Buil, X. Quelin, J.-P. Hermier, and B. Dubertret, “Towards non-blinking colloidal quantum dots” *Nat. Mater.*, vol. 7, pp. 659–664, 2008.

[35] H. Htoon, A. V Malko, D. Bussian, J. Vela, Y. Chen, J. A. Hollingsworth, and V. I. Klimov, “Highly Emissive Multiexcitons in Steady-State Photoluminescence of Individual ‘Giant’ CdSe/CdS Core/Shell Nanocrystals” *Nano Lett.*, vol. 10, pp. 2401–2407, 2010.

[36] M. Marceddu, M. Saba, F. Quochi, A. Lai, J. Huang, D. V Talapin, A. Mura, and G. Bongiovanni, “Charged excitons, Auger recombination and optical gain in CdSe/CdS nanocrystals” *Nanotechnology*, vol. 23, p. 015201, 2012.

[37] F. García-Santamaría, S. Brovelli, R. Viswanatha, J. a Hollingsworth, H. Htoon, S. a Crooker, and V. I. Klimov, “Breakdown of volume scaling in Auger recombination in CdSe/CdS heteronanocrystals: the role of the core-shell interface” *Nano Lett.*, vol. 11, pp. 687–693, 2011.

[38] Y.-S. Park, A. Malko, J. Vela, Y. Chen, Y. Ghosh, F. García-Santamaría, J. Hollingsworth, V. I. Klimov, and H. Htoon, “Near-Unity Quantum Yields of Biexciton Emission from CdSe/CdS Nanocrystals Measured

Using Single-Particle Spectroscopy" *Phys. Rev. Lett.*, vol. 106, pp. 187401, 2011.

[39] R. Osovsky, D. Cheskis, V. Kloper, A. Sashchiuk, M. Kroner, and E. Lifshitz, "Continuous-Wave Pumping of Multiexciton Bands in the Photoluminescence Spectrum of a Single CdTe-CdSe Core-Shell Colloidal Quantum Dot" *Phys. Rev. Lett.*, vol. 102, pp. 197401, 2009.

[40] D. Gachet, A. Avidan, I. Pinkas, and D. Oron, "An upper bound to carrier multiplication efficiency in type II colloidal quantum dots" *Nano Lett.*, vol. 10, pp. 164–170, 2010.

[41] D. Oron, M. Kazes, and U. Banin, "Multiexcitons in type-II colloidal semiconductor quantum dots" *Phys. Rev. B*, vol. 75, pp. 035330, 2007.

[42] J. B. Sambur, T. Novet, and B. a. Parkinson, "Multiple Exciton Collection in a Sensitized Photovoltaic System" *Science*, vol. 330, pp. 63–66, 2010.

[43] S. J. Kim, W. J. Kim, A. N. Cartwright, and P. N. Prasad, "Carrier multiplication in a PbSe nanocrystal and P3HT/PCBM tandem cell" *Appl. Phys. Lett.*, vol. 92, pp. 191107, 2008.

[44] V. I. Klimov, "Mechanisms for photogeneration and recombination of multiexcitons in semiconductor nanocrystals: implications for lasing and solar energy conversion" *J. Phys. Chem. B*, vol. 110, pp. 16827–16844, 2006.

[45] M. C. Hanna and a. J. Nozik, "Solar conversion efficiency of photovoltaic and photoelectrolysis cells with carrier multiplication absorbers" *J. Appl. Phys.*, vol. 100, pp. 074510, 2006.

[46] A. J. Nozik, M. C. Beard, J. M. Luther, M. Law, R. J. Ellingson, and J. C. Johnson, "Semiconductor quantum dots and quantum dot arrays and applications of multiple exciton generation to third-generation photovoltaic solar cells" *Chem. Rev.*, vol. 110, pp. 6873–6890, 2010.

[47] M. C. Beard, "Multiple exciton generation in semiconductor quantum dots" *J. Phys. Chem. Lett.*, vol. 2, pp. 1282–1288, 2011.

[48] V. Sukhovatkin, S. Hinds, L. Brzozowski, and E. H. Sargent, "Colloidal quantum-dot photodetectors exploiting multiexciton generation" *Science*, vol. 324, pp. 1542, 2009.

[49] X. Wang, X. Ren, K. Kahen, M. a Hahn, M. Rajeswaran, S. Maccagnano-Zacher, J. Silcox, G. E. Cragg, A. L. Efros, and T. D. Krauss, "Non-blinking semiconductor nanocrystals" *Nature*, vol. 459, pp. 686–689, 2009.

[50] Y. Louyer, L. Biadala, J.-B. Trebbia, M. J. Fernée, P. Tamarat, and B. Lounis, "Efficient biexciton emission in elongated CdSe/ZnS nanocrystals" *Nano Lett.*, vol. 11, pp. 4370–4375, 2011.

[51] R. D. Schaller, M. Sykora, S. Jeong, and V. I. Klimov, "High-efficiency carrier multiplication and ultrafast charge separation in semiconductor nanocrystals studied via time-resolved photoluminescence" *J. Phys. Chem. B*, vol. 110, pp. 25332–25338, 2006.

[52] J. J. H. Pijpers, E. Hendry, M. T. W. Milder, R. Fanciulli, J. Savolainen, J. L. Herek, D. Vanmaekelbergh, S. Ruhman, D. Mocatta, D. Oron, A. Aharoni, and U. Banin, "Carrier Multiplication and Its Reduction by Photodoping in Colloidal InAs Quantum Dots" *J. Phys. Chem. C*, vol. 111, pp. 4146–4152, 2007.

[53] J. J. H. Pijpers, E. Hendry, M. T. W. Milder, D. Vanmaekelbergh, S. Ruhman, D. Mocatta, D. Oron, A. Aharoni, U. Banin, and M. Bonn, "Additions and corrections 2008" *J. Phys. Chem. C*, vol. 112, pp. 4783–4784, 2008.

[54] G. Nair and M. G. Bawendi, "Carrier multiplication yields of CdSe and CdTe nanocrystals by transient photoluminescence spectroscopy" *Phys. Rev. B*, vol. 76, p. 081304, 2007.

[55] G. Nair, S. Geyer, L.-Y. Chang, and M. G. Bawendi, "Carrier multiplication yields in PbS and PbSe nanocrystals measured by transient photoluminescence" *Phys. Rev. B*, vol. 78, pp. 125325, 2008.

[56] J. A. Mcguire, M. Sykora, J. Joo, J. M. Pietryga, and V. I. Klimov, "Apparent versus true carrier multiplication yields in semiconductor nanocrystals" *Nano Lett.*, vol. 10, pp. 2049–2057, 2010.

[57] A. G. Midgett, H. W. Hillhouse, B. K. Hughes, A. J. Nozik, and M. C. Beard, "Flowing versus Static Conditions for Measuring Multiple Exciton Generation in PbSe Quantum Dots" *J. Phys. Chem. C*, vol. 114, pp. 17486–17500, 2010.

[58] F. Gesuele, M. Y. Sfeir, C. B. Murray, T. F. Heinz, and C. W. Wong, "Ultrafast Supercontinuum Spectroscopy of Carrier Multiplication and Biexcitonic Effects in Excited States of PbS Quantum Dots" *Nano Lett.*, vol. 12, pp. 2658–2664, 2012.

[59] L. A. Padilha, W. K. Bae, V. I. Klimov, J. M. Pietryga, and R. D. Schaller, "Response of semiconductor nanocrystals to extremely energetic excitation" *Nano Lett.*, vol. 13, pp. 925–932, 2013.

[60] A. Sitt, F. Della Sala, G. Menagen, and U. Banin, "Multiexciton engineering in seeded core/shell nanorods: transfer from type-I to quasi-type-II regimes" *Nano Lett.*, vol. 9, pp. 3470–3476, 2009.

[61] J. Zhao, O. Chen, D. B. Strasfeld, and M. G. Bawendi, "Biexciton Quantum Yield Heterogeneities in Single CdSe (CdS) Core (Shell) Nanocrystals and Its Correlation to Exciton Blinking" *Nano Lett.*, vol. 12, pp. 4477–4483, 2012.

[62] I. Gdor, H. Sachs, A. Roitblat, D. B. Strasfeld, M. G. Bawendi, and S. Ruhman, "Exploring Exciton Relaxation and Multiexciton Generation in PbSe Nanocrystals Using Hyperspectral Near-IR Probing" *ACS Nano*, vol. 6, pp. 3269–3277, 2012.

[63] C. Galland, Y. Ghosh, A. Steinbrück, J. a Hollingsworth, H. Htoon, and V. I. Klimov, "Lifetime blinking in nonblinking nanocrystal quantum dots" *Nat. Commun.*, vol. 3, pp. 908, 2012.

[64] P. P. Jha and P. Guyot-Sionnest, "Trion Decay in Colloidal Quantum Dots" *ACS Nano*, vol. 3, pp. 1011–1015, 2009.

[65] S. F. Wuister, R. Koole, C. D. M. Donega, and A. Meijerink, "Temperature-Dependent Energy Transfer in Cadmium Telluride Quantum Dot Solids" *J. Appl. Phys.*, vol. 109, pp. 5504, 2005.

[66] O. Labeau, P. Tamarat, and B. Lounis, "Temperature Dependence of the Luminescence Lifetime of Single CdSe/ZnS Quantum Dots" *Phys. Rev. Lett.*, vol. 90, p. 257404, 2003.

[67] H.-J. Eisler, V. C. Sundar, M. G. Bawendi, M. Walsh, H. I. Smith, and V. I. Klimov, "Color-selective semiconductor nanocrystal laser" *Appl. Phys. Lett.*, vol. 80, pp. 4614, 2002.

[68] M. Kazes, D. Oron, I. Shweky, and U. Banin, “Temperature Dependence of Optical Gain in CdSe/ZnS Quantum Rods” *J. Phys. Chem. C*, vol. 111, pp. 7898–7905, 2007.

[69] L. Pavesi, L. Dal Negro, C. Mazzoleni, G. Franzò, and F. Priolo, “Optical gain in silicon nanocrystals” *Nature*, vol. 408, pp. 440–444, 2000.

[70] Y. Chen, J. Herrnsdorf, B. Guilhabert, Y. Zhang, I. M. Watson, E. Gu, N. Laurand, and M. D. Dawson, “Colloidal quantum dot random laser” *Opt. Exp.*, vol. 19, pp. 2996–3003, 2011.

[71] Y. Shirasaki, G. J. Supran, M. G. Bawendi, and V. Bulović, “Emergence of colloidal quantum-dot light-emitting technologies” *Nat. Photon.*, vol. 7, pp. 13–23, 2013.

[72] S. Nizamoglu, G. Zengin, and H. V. Demir, “Color-converting combinations of nanocrystal emitters for warm-white light generation with high color rendering index” *Appl. Phys. Lett.*, vol. 92, pp. 031102, 2008.

[73] S. Coe, W.-K. Woo, M. G. Bawendi, and V. Bulović, “Electroluminescence from single monolayers of nanocrystals in molecular organic devices” *Nature*, vol. 420, pp. 800–803, 2002.

[74] R. Krahne, M. Zavelani-Rossi, M. G. Lupo, L. Manna, and G. Lanzani, “Amplified spontaneous emission from core and shell transitions in CdSe/CdS nanorods fabricated by seeded growth” *Appl. Phys. Lett.*, vol. 98, pp. 063105, 2011.

[75] Y. Liao, G. Xing, N. Mishra, T. C. Sum, and Y. Chan, “Low threshold, amplified spontaneous emission from core-seeded semiconductor nanotetrapods incorporated into a sol-gel matrix” *Adv. Opt. Mat.*, vol. 24, pp. 159–164, 2012.

[76] Y. Chen, B. Guilhabert, J. Herrnsdorf, Y. Zhang, A. R. Mackintosh, R. a. Pethrick, E. Gu, N. Laurand, and M. D. Dawson, “Flexible distributed-feedback colloidal quantum dot laser” *Appl. Phys. Lett.*, vol. 99, pp. 241103, 2011.

[77] Y. Chan, J.-M. Caruge, P. T. Snee, and M. G. Bawendi, “Multiexcitonic two-state lasing in a CdSe nanocrystal laser” *Appl. Phys. Lett.*, vol. 85, pp. 2460, 2004.

[78] Y. Chan, J. S. Steckel, P. T. Snee, J.-M. Caruge, J. M. Hodgkiss, D. G. Nocera, and M. G. Bawendi, "Blue semiconductor nanocrystal laser" *Appl. Phys. Lett.*, vol. 86, pp. 073102, 2005.

[79] J. J. Jasieniak, I. Fortunati, S. Gardin, R. Signorini, R. Bozio, A. Martucci, and P. Mulvaney, "Highly Efficient Amplified Stimulated Emission from CdSe-CdS-ZnS Quantum Dot Doped Waveguides with Two-Photon Infrared Optical Pumping" *Adv. Mat.*, vol. 20, pp. 69–73, 2008.

[80] F. Todescato, I. Fortunati, S. Gardin, E. Garbin, E. Collini, R. Bozio, J. J. Jasieniak, G. Della Giustina, G. Brusatin, S. Toffanin, and R. Signorini, "Soft-Lithographed Up-Converted Distributed Feedback Visible Lasers Based on CdSe-CdZnS-ZnS Quantum Dots" *Adv. Func. Mat.*, vol. 22, pp. 337–344, 2012.

[81] R. Signorini, I. Fortunati, F. Todescato, S. Gardin, R. Bozio, J. J. Jasieniak, A. Martucci, G. Della Giustina, G. Brusatin, and M. Guglielmi, "Facile production of up-converted quantum dot lasers" *Nanoscale*, vol. 3, pp. 4109–4113, 2011.

[82] C. Zhang, F. Zhang, T. Zhu, A. Cheng, J. Xu, Q. Zhang, S. E. Mohney, R. H. Henderson, and Y. A. Wang, "Two-photon-pumped lasing from colloidal nanocrystal quantum dots" *Opt. Lett.*, vol. 33, pp. 2437–2439, 2008.

[83] D. R. Larson, W. R. Zipfel, R. M. Williams, S. W. Clark, M. P. Bruchez, F. W. Wise, and W. W. Webb, "Water-soluble quantum dots for multiphoton fluorescence imaging in vivo" *Science*, vol. 300, pp. 1434–1436, 2003.

[84] Q. Zheng, G. S. He, and P. N. Prasad, "A novel near IR two-photon absorbing chromophore: Optical limiting and stabilization performances at an optical communication wavelength" *Chem. Phys. Lett.*, vol. 475, pp. 250–255, 2009.

[85] G. L. Dakovski and J. Shan, "Size dependence of two-photon absorption in semiconductor quantum dots" *J. Appl. Phys.*, vol. 114, pp. 014301, 2013.

[86] G. Xing, Y. Liao, X. Wu, S. Chakrabortty, X. Liu, E. K. L. Yeow, Y. Chan, and T. C. Sum, "Ultralow-Threshold Two-Photon Pumped

Amplified Spontaneous Emission and Lasing from Seeded CdSe/CdS Nanorod Heterostructures" *ACS Nano*, vol. 6, pp. 10835–10844, 2012.

[87] A. F. Cihan, Y. Kelestemur, B. Guzelturk, U. Kurum, H. G. Yaglioglu, A. Elmali, and H. V. Demir "Attractive versus Repulsive Excitonic Interactions of Colloidal Quantum Dots Control Blue- to Red-Shifting (and Non-Shifting) Amplified Spontaneous Emission" *submitted*, 2013.

[88] A. Piryatinski, S. A. Ivanov, S. Tretiak, and V. I. Klimov, "Effect of Quantum and Dielectric Confinement on the Exciton − Exciton Interaction Energy in Type II Core / Shell Semiconductor Nanocrystals" *Nano Lett.*, vol. 7, pp. 108–115, 2007.

[89] J. Nanda, S. A. Ivanov, H. Htoon, I. Bezel, A. Piryatinski, S. Tretiak, and V. I. Klimov, "Absorption cross sections and Auger recombination lifetimes in inverted Core-Shell nanocrystals: Implications for lasing performance" *J. Appl. Phys.*, vol. 99, p. 034309, 2006.

[90] L. P. Balet, S. A. Ivanov, A. Piryatinski, M. Achermann, and V. I. Klimov, "Inverted Core/Shell Nanocrystals Continuously Tunable between Type-I and Type-II Localization Regimes" *Nano Lett.*, vol. 4, pp. 1485–1488, 2004.

[91] R. Cooney, S. Sewall, D. Sagar, and P. Kambhampati, "Gain Control in Semiconductor Quantum Dots via State-Resolved Optical Pumping" *Phys. Rev. Lett.*, vol. 102, p. 127404, 2009.

[92] M. Saba, S. Minniberger, F. Quochi, J. Roither, M. Marceddu, A. Gocalinska, M. V. Kovalenko, D. V. Talapin, W. Heiss, A. Mura, and G. Bongiovanni, "Exciton-Exciton Interaction and Optical Gain in Colloidal CdSe/CdS Dot/Rod Nanocrystals" *Adv. Mater.*, vol. 21, pp. 4942–4946, 2009.

[93] F. García-Santamaría, Y. Chen, J. Vela, R. D. Schaller, J. A. Hollingsworth, and V. I. Klimov, "Suppressed Auger recombination in 'giant' nanocrystals boosts optical gain performance" *Nano Lett.*, vol. 9, pp. 3482–3488, 2009.

[94] J. W. Haus, H. S. Zhou, I. Honma, and H. Komiyama, "Quantum confinement in semiconductor heterostructure nanometer-size particles" *Phys. Rev. B*, vol. 47, pp. 1359–1365, 1993.

[95] J. Nanda, S. A. Ivanov, M. Achermann, I. Bezel, A. Piryatinski, and V. I. Klimov, "Light Amplification in the Single-Exciton Regime Using Exciton-Exciton Repulsion in Type-II Nanocrystal Quantum Dots" *J. Phys. Chem. C*, vol. 111, pp. 15382–15390, 2007.

[96] S. A. Ivanov, J. Nanda, A. Piryatinski, M. Achermann, L. P. Balet, I. V. Bezel, P. O. Anikeeva, S. Tretiak, and V. I. Klimov, "Light Amplification Using Inverted Core/Shell Nanocrystals: Towards Lasing in the Single-Exciton Regime" *J. Phys. Chem. B*, vol. 108, pp. 10625–10630, 2004.

[97] J. Muller, J. M. Lupton, P. G. Lagoudakis, F. Schindler, R. Koeppe, A. L. Rogach, J. Feldmann, D. V Talapin, and H. Weller, "Wave Function Engineering in Elongated Semiconductor Nanocrystals with Heterogeneous Carrier Confinement" *Nano Lett.*, vol. 5, pp. 2044–2049, 2005.

[98] G. Xing, S. Chakrabortty, K. L. Chou, N. Mishra, C. H. A. Huan, Y. Chan, and T. C. Sum, "Enhanced tunability of the multiphoton absorption cross-section in seeded CdSe/CdS nanorod heterostructures" *Appl. Phys. Lett.*, vol. 97, pp. 061112, 2010.

[99] M. Zavelani-Rossi, M. G. Lupo, R. Krahne, L. Manna, and G. Lanzani, "Lasing in self-assembled microcavities of CdSe/CdS core/shell colloidal quantum rods" *Nanoscale*, vol. 2, pp. 931–935, 2010.

[100] D. V. Talapin, R. Koeppe, S. Go, A. Kornowski, J. M. Lupton, A. L. Rogach, O. Benson, J. Feldmann, and H. Weller, "Highly Emissive Colloidal CdSe / CdS Heterostructures of Mixed Dimensionality" *Nano Lett.*, vol. 3, pp. 1677–1681, 2003.

[101] A. F. Cihan, P. L. Hernandez-Martinez, Y. Kelestemur, E. Mutlugun, and H. V. Demir, "Observation of Biexcitons in Nanocrystal Solids in the Presence of Photocharging" *ACS Nano*, vol. 7, pp. 4799-4809, 2013.

[102] A. L. Rogach, Ed., *Semiconductor Nanocrystal Quantum Dots*. Wien, Austria: Springer-Verlag, 2008.

[103] G. Rainò, T. Stoferle, I. Moreels, R. Gomes, J. S. Kamal, Z. Hens, and R. F. Mahrt, "Probing the Wave Function Delocalization in CdSe/CdS Dot-in-Rod Nanocrystals by Time- and Temperature-Resolved Spectroscopy" *ACS Nano*, vol. 5, pp. 4031–4036, 2011.

[104] L. P. Balet, S. a. Ivanov, A. Piryatinski, M. Achermann, and V. I. Klimov, “Inverted Core/Shell Nanocrystals Continuously Tunable between Type-I and Type-II Localization Regimes” *Nano Lett.*, vol. 4, pp. 1485–1488, 2004.

[105] I. Moreels, G. Rainò, R. Gomes, Z. Hens, T. Stöferle, and R. F. Mahrt, “Nearly temperature-independent threshold for amplified spontaneous emission in colloidal CdSe/CdS quantum dot-in-rods” *Adv. Opt. Mater.*, vol. 24, pp. 231–235,. 2012.

[106] G. Rainò, T. Stoferle, I. Moreels, R. Gomes, Z. Hens, and R. F. Mahrt, “Controlling the Exciton Fine Structure Splitting in CdSe / CdS Dot-in-Rod” *ACS Nano*, vol. 6, pp. 1979–1987, 2012.

[107] D. V Talapin, J. H. Nelson, E. V Shevchenko, S. Aloni, B. Sadtler, and a P. Alivisatos, “Seeded growth of highly luminescent CdSe/CdS nanoheterostructures with rod and tetrapod morphologies” *Nano Lett.*, vol. 7, pp. 2951–2959, 2007.

[108] A. F. Cihan, Y. Kelestemur, B. Guzelturk, and H. V. Demir, “Type Tunable Amplified Spontaneous Emission from Core Seeded CdSe/CdS Core/Shell Nanorods via Exciton-Exciton Engineering” *submitted*, 2013.

[109] C. De Mello Donegá, M. Bode, and A. Meijerink, “Size- and temperature-dependence of exciton lifetimes in CdSe quantum dots” *Phys. Rev. B*, vol. 74, p. 085320, 2006.

[110] R. D. Schaller, M. a. Petruska, and V. I. Klimov, “Effect of electronic structure on carrier multiplication efficiency: Comparative study of PbSe and CdSe nanocrystals” *Appl. Phys. Lett.*, vol. 87, pp. 253102, 2005.

[111] X. Zhu, “Exceeding the Limit in Solar Energy Conversion with Multiple Excitons” *Acc. Chem. Res.*, vol. 46, pp. 1239–1241, 2013.

[112] V. Lesnyak, A. Lutich, N. Gaponik, M. Grabolle, A. Plotnikov, U. Resch-Genger, and A. Eychmüller, “One-pot aqueous synthesis of high quality near infrared emitting Cd1−xHgxTe nanocrystals” *J. Mat. Chem.*, vol. 19, pp. 9147–9152, 2009.

[113] A. Franceschetti, J. M. An, and A. Zunger, “Impact ionization can explain carrier multiplication in PbSe quantum dots” *Nano Lett.*, vol. 6, pp. 2191–2195, 2006.

[114] A. F. Cihan, S. Akhavan, and H. V. Demir, “Multiple exciton generation and charge accumulation from photosensors of CdHgTe monolayer nanocrystals” *submitted*, 2013.

[115] S. Akhavan, B. Guzelturk, V. K. Sharma, and H. V. Demir, “Large-area semi-transparent light-sensitive nanocrystal skins” *Opt. Exp.*, vol. 20, pp. 25255–25266, 2012.

[116] S. Akhavan, K. Gungor, E. Mutlugun, and H. V. Demir, “Plasmonic light-sensitive skins of nanocrystal monolayers” *Nanotechnology*, vol. 24, pp. 155201, 2013.

[117] A. Shavel, N. Gaponik, and A. Eychmüller, “The assembling of semiconductor nanocrystals” *Eur. J. Inorg. Chem.*, pp. 3613–3623, 2005.